Numerical simulations of shocks and interfaces in highly compressible multiphase and multicomponent flows

by

Marc T. Henry de Frahan

Dissertation Proposal Exam
October 2015

Doctoral Committee:

Assistant Professor Eric Johnsen, Chair
Professor David R. Dowling
Professor R. Paul Drake
Associate Professor Krzysztof J. Fidkowski

ACKNOWLEDGEMENTS

This research was supported in part by the DOE NNSA/ASC under the predictive Science Academic Alliance Program by Grant No. DEFC52-08NA28616, by ONR grant N00014-12-1-0751 under Dr. Ki-Han Kim, by NSF grant CBET 1253157, by the Rackham Predoctoral Fellowship at the University of Michigan, and through computational resources and services provided by Advanced Research Computing at the University of Michigan, Ann Arbor. This work used the Extreme Science and Engineering Discovery Environment (XSEDE), which is supported by National Science Foundation grant number OCI-1053575.

TABLE OF CONTENTS

LIST OF FIGURES

Figure

ABSTRACT

Numerical simulations of shocks and interfaces in highly compressible multiphase and multicomponent flows
by
Marc T. Henry de Frahan

Chair: Eric Johnsen

Developing a highly accurate numerical framework to study multiphase mixing in high speed flows containing shear layers, shocks, and strong accelerations is critical to many scientific and engineering endeavors. These flows occur across a wide range of scales: from tiny bubbles in human tissue to massive stars collapsing. The lack of understanding of these flows has impeded the success of many engineering applications, our comprehension of astrophysical and planetary formation processes, and the development of biomedical technologies. Controlling mixing between different fluids is central to achieving fusion energy, where mixing is undesirable, and supersonic combustion, where enhanced mixing is important. Iron, found throughout the universe and a necessary component for life, is dispersed through the mixing processes of a dying star. Non-invasive treatments using ultrasound to induce bubble collapse in tissue are being developed to destroy tumors or deliver genes to specific cells. Laboratory experiments of these flows are challenging because the initial conditions and material properties are difficult to control, modern diagnostics are unable to resolve the flow dynamics and conditions, and experiments of these flows are expensive. Numerical simulations can circumvent these difficulties and, therefore, have become a necessary component of any scientific challenge.

We present advances in the three fields of numerical methods, high performance computing, and multiphase flow modeling: (i) novel numerical methods to capture accurately the multiphase nature of the problem; (ii) modern high performance computing paradigms to resolve the disparate time and length scales of the physical processes; (iii) new insights and models of the dynamics of multiphase flows, including mixing through hydrodynamic instabilities.

The Discontinuous Galerkin (DG) method has been shown to be a highly scalable, geometrically flexible, high-order accurate numerical method to solve systems of partial differential equations. This powerful method had not been adapted to multiphase flows. Conventional implementation of this method to multiphase flows resulted in numerical errors that led to incorrect solutions or simulation failures. We present a new procedure in the DG method which preserves the high-order accuracy while

avoiding these numerical errors. This method is coupled to numerical sensors which detect flow discontinuities to apply limiting procedures only where necessary and retain broadband motions in smooth regions of the flow. We also present solution enhancement techniques to increase the order of accuracy of the method without increasing the numbers of degrees of freedom. Our method has been validated with the usual numerical tests as well as through comparisons with theory and experiments of hydrodynamic instabilities as well as experiments of a shock in air hitting a drop of water.

Our efficient numerical method must be coupled to a state-of-the-art parallel paradigm to resolve all the flow features. We use Graphics Processing Units (GPU), traditionally used to manipulate computer graphics, to perform fast, computationally intensive, and highly parallel vector operations. Since on-chip GPU memory is limited, the problem must be distributed across multiple GPUs and the data must be moved efficiently across the network to minimize communication costs. We developed a multi-GPU parallel code which uses the Message Passing Interface to communicate between GPUs. We show excellent weak and strong scaling. This work presents a viable path towards exascale computing.

Using this computational framework, we provide key insights into the dynamics of multiphase flows relevant to engineering, basic science, and biomedical applications. We analyze shocks interacting with multiple layers of different materials and show how to control the level of mixing by varying the material composition, material ordering, material thickness, and perturbation phase alignment. This result is key to many engineering applications involving flows with shocks and multiple fluids where controlling mixing is important (*e.g* fusion energy and supersonic combustion). We explore the use of the Rayleigh-Taylor instability to characterize the strength of metals at extreme pressures and strain-rates. In this case, simulations and experiments are compared to validate theoretical models of material strength. Finally, we study shocks interacting with bubbles and drops, supersonic drops hitting rigid walls, and blast waves interacting with perturbed interfaces. We show how mixing dynamics affect the evolution of complex interfacial multiphase flows. These studies have direct applications to engineering and biomedical fields such as fuel injection problems, plasma deposition, cancer treatments, and turbomachinery.

CHAPTER I

Introduction

The objective of this chapter is to define the scope of this dissertation thesis and emphasize the importance and relevance of this work to many scientific and engineering problems. We start by defining and exploring the key concepts involved in this work, particularly mixing in compressible multiphase flows and phenomena at interfaces. We then explain the context of this work and relevance to several applications, focusing primarily on inertial confinement fusion and supernova collapse. Finally, we conclude this chapter by presenting our objective, thesis outline, and the main contributions of this work.

1.1 Physical context

Gases, liquids, and plasmas belong to the general family of fluids, *i.e.* they are substances that change shape and deform continuously, they are said to *flow*, under the effect of a force. Fluid flows are observed throughout nature and span many length scales, from the blood in our veins to the interstellar medium. Due to their prevalence, understanding fluid flows is critical to many applications. The study of single fluid flows, flows where there is only one type of fluid in a particular state, e.g. the flow of air over an airplane wing, has led to countless breakthroughs in scientific, engineering, and medical fields.

This thesis focuses on more complex flows, flows which contain multiple types of fluid. *Multifluid flows* are flows which involve the interactions of fluids in the same phase. These flows occur, for example, when different types of liquids are in the same system. Pouring honey into hot tea, for example, involves two liquids with different temperatures, densities, and viscosities. Multifluid flows are generally more difficult to analyze than singlefluid flows because the differences in the fluid material properties have a strong effect on the flow dynamics.

Many of the flows we discuss pertain to multifluid flows, particularly flows with different gases. However, the tools developed and several flows studied in this thesis are applied to *multiphase flows*, a broader class of flows in which fluids in different phases are present. The injection of fuel, a liquid spray, into a car's combustion chamber filled with hot gases, is an example of a multiphase flow. The scope of this work is restricted to multiphase flows where fluids are not actively changing phases,

e.g going from a liquid phase to a gaseous one. We focus instead on the numerical treatment of multiphase flows and the study of several specific multiphase flows.

Particularly, we discuss *compressible* multiphase flows, where there are local changes in density, high pressure regions, and velocities at significant fractions of the speed of sound. The equations typically used to model compressible flows are the Euler equations, a set of hyperbolic conservation laws for mass, momentum, and energy. The Euler equations are a valid approximation for flows where viscosity, as well as other diffusive effects, are negligible. The Reynolds number, defined as the ratio of inertial forces to viscous forces, is used to determine the validity of this assumption. A high Reynolds number is indicative of a flow which may be modeled using the Euler equations. Other forces, e.g. surface tension and electro-magnetic forces, must also be small in comparison to inertial forces. The Euler equations are scale invariant. This same system of equations can be used to describe systems across a wide range of scales, from millimeters to light years, allowing for the design of laboratory experiments that can accurately represent the physical phenomena at astrophysical scales.

1.2 Mixing in compressible multiphase flows

In this thesis, we concentrate on phenomena at interfaces between fluids in compressible multiphase flows. The particular phenomena important to the applications of interest, described in Section 1.3, are *hydrodynamic instabilities*. These are particularly important as they initiate mixing between different fluids, determine the evolution and amount of mixing, and thus directly influence the overall flow dynamics. Hydrodynamic instabilities occur when small perturbations on an interface between fluids grow because of the dynamics of the flow. The process behind the perturbation growth dictates the nature and type of instability.

1.2.1 Richtmyer-Meshkov instability

The Richtmyer-Meshkov instability occurs when a shock traverses a perturbed interface between fluids of different densities [1, 2]. The growth of the perturbation is due to the shock generating baroclinic vorticity at the interface [3]. Specifically, the vorticity is created by the misalignement of the pressure gradient across the shock and the density gradient across the interface, as illustrated by the last term in the vorticity evolution equation for a compressible inviscid flow,

$$\frac{\partial \boldsymbol{\omega}}{\partial t} + \mathbf{u} \cdot \nabla \boldsymbol{\omega} = (\boldsymbol{\omega} \cdot \nabla)\mathbf{u} - \boldsymbol{\omega} \nabla \cdot \mathbf{u} + \frac{1}{\rho^2}(\nabla \rho \times \nabla p) \tag{1.1}$$

where ρ is the density, p is the pressure, $\mathbf{u}$ is the velocity, and $\boldsymbol{\omega} = \nabla \times \mathbf{u}$ is the vorticity. Vortex stretching, the first term on the right hand side, only appears in three-dimensional flows. Vortex compression, the second term, includes compressibility effects.

When the shock interacts with the interface, it first compresses the perturbations.

If the shock is moving into a lighter fluid ($\nabla p \cdot \nabla \rho > 0$), it induces a phase inversion in the perturbation. After the shock has left the interface, the only mechanism left to drive the interface growth is the vortex sheet at the interface formed by baroclinic vorticity generation, Figure 1.1. As such, the Richtmyer-Meshkov instability is not a classical instability because it does not exhibit exponential linear growth and does not contain any feedback mechanisms.[1] The vortex sheet induces different velocities at different points along the interface. These velocities deform the interface and create a bubble, defined as the light fluid moving into the heavier fluid, and a spike – a heavy fluid moving into lighter fluid.

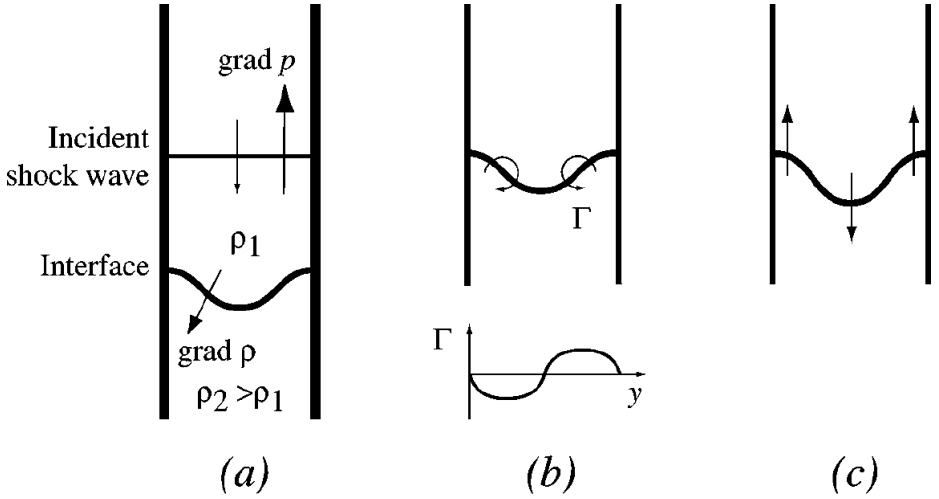

Figure 1.1: Illustration of a Richtmyer-Meshkov unstable flow for the vorticity generated at a light/heavy interface. a) Initial condition. b) Circulation at the interface and vortex sheet strength. c) Perturbation growth. From Brouillette [3].

The Richtmyer-Meshkov instability has been extensively studied in the past. Initial growth models were proposed by Richtmyer [1], Meyer [4]. These models use Rayleigh-Taylor instability perturbation analysis with an impulsive acceleration. They are valid at early time and predict a constant growth rate. Other perturbation models have since been proposed for the entire growth of the perturbation. The most successful ones are those by Zhang and Sohn [5] and Sadot et al. [6]. This latter one is in very good agreement with experiments. Another modeling approach focuses on modeling the vorticity deposition and deforming the interface based on vortex sheet evolution equations. Samtaney and Zabusky [7], Jacobs and Sheeley [8] evaluated the strength of the vortex sheet and used it to predict the perturbation growth. Experimental and numerical studies of the Richtmyer-Meshkov instability have been performed extensively to explore many different configurations, effects, and regimes, [3].

[1]To stay consistent with the literature, we will keep calling it an instability. We should really be referring to the Richtmyer-Meshkov process.

1.2.2 Rayleigh-Taylor instability

The Rayleigh-Taylor instability occurs when a heavy fluid is accelerated into a lighter one. A classic example of this instability is when a heavy fluid is above a light fluid in a gravitational field. The gravitational acceleration amplifies the perturbations at the interface between the fluids, making spikes of heavy fluid fall and bubbles of light fluid rise, Figure 1.2. The perturbation growth in the Rayleigh-Taylor instability is driven by buoyancy.

Taylor [9] predicted the exponential growth of the perturbations in the early phase of the instability, when the perturbation can still be described using normal mode analysis. In the non-linear regime, the growth is best described as bubbles rising and spikes falling quadratically in time, according to

$$h_{b/s} = \alpha_{b/s} A g t^2 \tag{1.2}$$

where h is the height of the bubble/spike, A is the Atwood number, g is the acceleration, and t is the time. In recent years, a lot of work in this field has been focused on measuring the model constants $\alpha_{b/s}$ [10, 11, 12, 13, 14, 15, 16]. For time-varying accelerations, buoyancy-drag models have been developed to predict the instability growth [17, 18, 19]. These models look at the momentum balance of a bubble of light fluid rising in a heavier one and consider buoyancy and drag forces on the bubble (or spike). In general, as the instability develops, the growth region transitions to a turbulent mixing region. This transition to turbulence is an active research area today [20].

Figure 1.2: Slightly denser dyed water spikes fall in water due to the Rayleigh-Taylor instability. Experimental pictures by James Riordon, AIP.

1.2.3 Kelvin-Helmholtz instability

Though relevant to many of the flows of interest, we will not discuss the Kelvin-Helmholtz instability in depth. The Kelvin-Helmholtz instability occurs at the interface between fluids where there is a velocity gradient across the interface. This typically happens in shear flows where fluids are moving parallel to each other at different speeds, Figure 1.3. For example, the interface of a fluid injected into a quiescent fluid is Kelvin-Helmholtz unstable. The Kelvin-Helmholtz instability can also be seen in the shear flows in the massive storm near Jupiter's Great Red Spot, Figure 1.4. The late-time roll-ups near the bubble and spike observed in the Richtmyer-Meshkov and Rayleigh-Taylor instabilities are due to the Kelvin-Helmholtz instability.

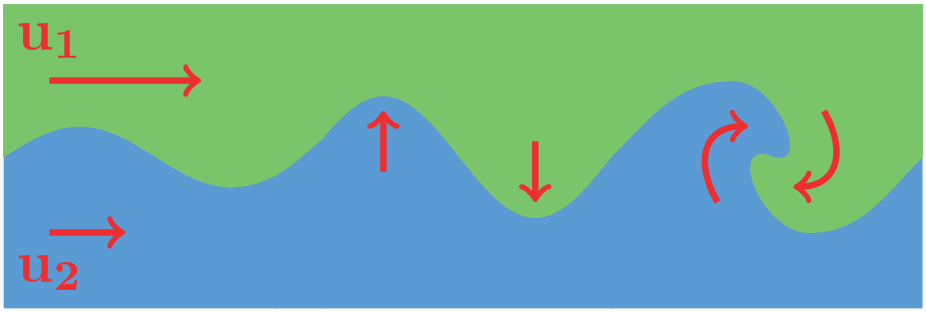

Figure 1.3: Illustration of a Kelvin-Helmholtz unstable flow. The fluid on the top is moving at a different velocity than the fluid on the bottom. In this shear flow configuration, the perturbations at the interface are Kelvin-Helmholtz unstable and will grow accordingly, thereby mixing the two fluids.

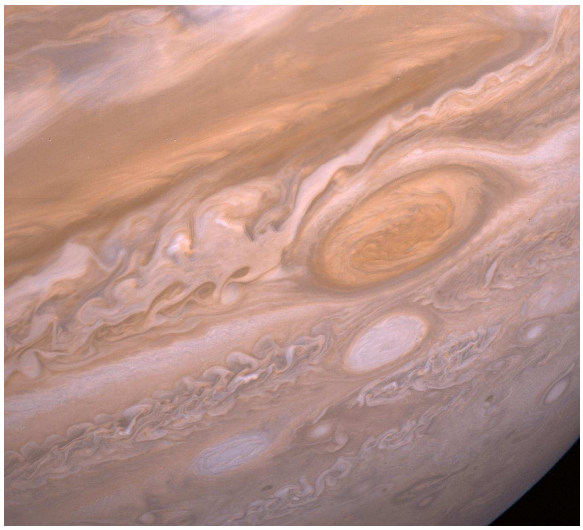

Figure 1.4: Shear flow in the storm near Jupiter's Great Red Spot have created a large scale example of the Kelvin-Helmholtz instability. Image of Jupiter from Voyager 2 flyby. Photo credit: National Aeronautics and Space Administration.

1.3 Scientific and engineering applications

Compressible multiphase flows are ubiquitous in science and engineering. Mitigating cavitation erosion, which involves small air bubbles created by tensile forces in the wake of a ship's propeller collapsing violently and damaging the propeller, is crucial to many naval engineers [21]. For high speed multiphase nozzle injection, such as variable phase turbines used in geothermal waste heat recovery systems [22, 23], understanding liquid droplet breakup in supersonic flow is important for developing liquid atomizations models [24]. In manufacturing, plasma deposition is a technique in which thin films of solid are deposited using a vaporized liquid. The gas and liquid droplets usually travel at high velocities, and understanding their impact on the substrate is important for controlling surface roughness and defects [25, 26]. In car engines, the liquid fuel is injected as a high speed spray into the combustion chamber. Efficient mixing of the fuel and oxygen is important to minimize particulates and maximize the combustion rate and, thus, fuel efficiency [27]. In supersonic combustion ramjets, or scram-jets, a type of jet engine for hypersonic flight, increasing the rate of mixing between the fuel and oxidizer is critical to the engine's success as the typical residence time in the combustion chamber is milliseconds [28]. Shock induced mixing has been proposed as an efficient mixing method for accomplishing this [28].

In the biomedical sciences, therapies have been developed where flows of complex tissues interacting with high pressure waves are prevalent. In shockwave lithotripsy [29], a common technique for treating kidney stones, external acoustic pulses are used to crush the kidney stones in the patient. Histotripsy uses ultrasound to induce tissue necrosis and tissue fractionation to treat cancer tumors [30]. These non-invasive therapy tools focus energy into tissue and create pressure waves interacting with interfaces of different materials.

At much larger scales, though usually at lower speeds, terrestrial flows, like atmospheric inversions [31], magma flow and solidification [32], and ocean mixing due to sudden temperature changes [33], can also be subject to mixing instabilities such as the Kelvin-Helmholtz and Rayleigh-Taylor instabilities. Planetary formation processes and planetary object collisions are governed by flows in which shocks are interacting with fluids in different phases [34].

Of particular interest to this thesis and a specific focus and application of this work is inertial confinement fusion and supernovae.

1.3.1 Inertial confinement fusion

Inertial confinement fusion (ICF) is a technology for harnessing energy from fusion reactions to generate electricity using a nearly unlimited source of material, hydrogen, without producing carbon products [35]. In ICF, a gaseous deuterium and tritium fuel is encased in a small spherical capsule, about 5 mm in diameter. The capsule's shell, the ablator, is primarily plastic doped with several other elements, Figure 1.5. It is heated to very high temperatures using various energy sources. For indirect drive ICF, as pursued at the National Ignition Facility at Lawrence Livermore National Laboratory, the capsule is suspended inside a gold canister, called a hohlraum. One

hundred and ninety two laser beams are aimed at the inner hohlraum walls, Figure 1.5 and the laser light is converted to x-rays by the gold walls. The x-rays then uniformly bathe the capsule with intense radiation and ablate the outer shell of the capsule. The outer shell explodes outward and, by conservation of momentum (sometimes referred to, in this context, as the "rocket effect"), the inner deuterium-tritium fuel is compressed. Temperatures can reach several tens of millions of degrees [36]. At these temperatures, the compressed fuel in the core is expected to undergo thermonuclear burn and produce helium and very energetic neutrons.

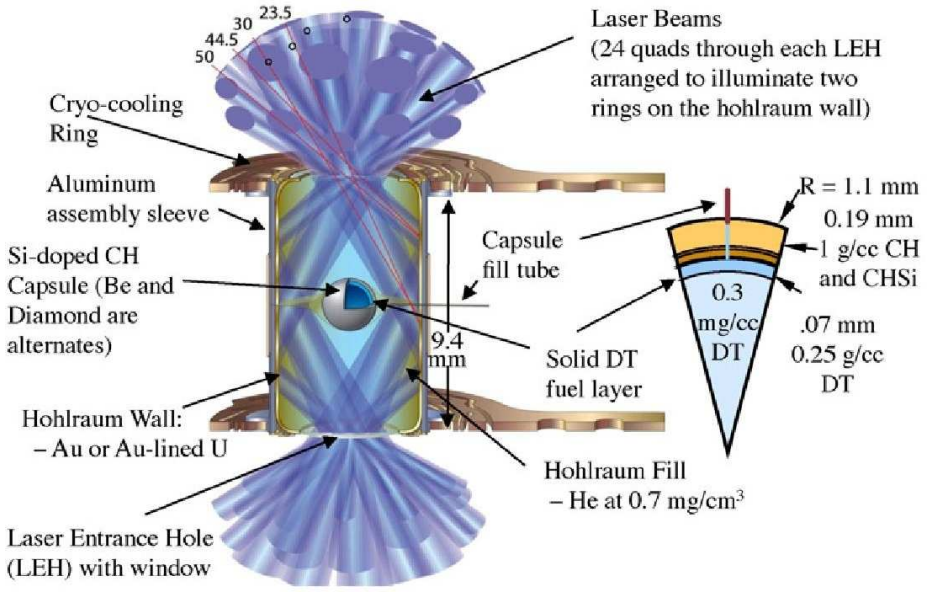

Figure 1.5: Indirect drive ICF schematic of the hohlraum (left) and fuel capsule (right). From Landen et al. [37].

One of the key challenges in ICF is achieving the very high densities and temperatures necessary for initiating thermonuclear burn. This imposes very tight constraints on the sphericity of the compression, *i.e.* a non-spherical implosion will not compress the fuel to high enough temperatures in center of the capsule, the hotspot. Hydrodynamic instabilities, such as the Kelvin-Helmholtz, Rayleigh-Taylor, and Richtmyer-Meshkov instabilities, significantly perturb the uniform compression and induce mixing between the hot fuel and the relatively cold outer shell of the capsule. The mixing reduces the temperature in the hotspot and inhibits ignition. Mixing through hydrodynamic instabilities is a main reason for the failure of current fusion efforts [38].

1.3.2 Core collapse supernovae

At the other end of the length scale spectrum, core collapse supernovae form the biggest explosion in the universe, Figure 1.6. During the life of a star, nuclear fusion in the star manufactures progressively heavier elements [39, 40]. Eventually, an iron core forms and fusion reactions no longer release energy to power the next sequence

of fusion reactions. Further reactions contribute to reducing the core's pressure. Throughout this process, gravitational forces create an onion-like series of layers with the lightest elements, like hydrogen and helium, on the outside and the heaviest elements, like silicon and iron, towards the center, Figure 1.7. The supernova occurs when the core becomes so massive that thermal and radiation forces in the core are overwhelmed by gravitational forces. The core then collapses at velocities approaching a quarter of the speed of light. During the explosion, the supernova generates, in the span of several seconds, a large amount of neutrons. Through the r-process, a neutron capture mechanism, approximately half the amount of elements above iron in the universe are created [41, 42]. Depending on the type of supernova, the core may rebound upon collapse and produce a powerful blast wave which interacts with the many different layers of material. This process initiates mixing of the elements through the Rayleigh-Taylor, Kelvin-Helmholtz, and Richtmyer-Meshkov instabilities [38]. These processes occurring during a supernova explosion are responsible for dispersing these elements in the interstellar medium where gravitational forces will slowly coalesce the dispersed elements to forms new stars and planets.

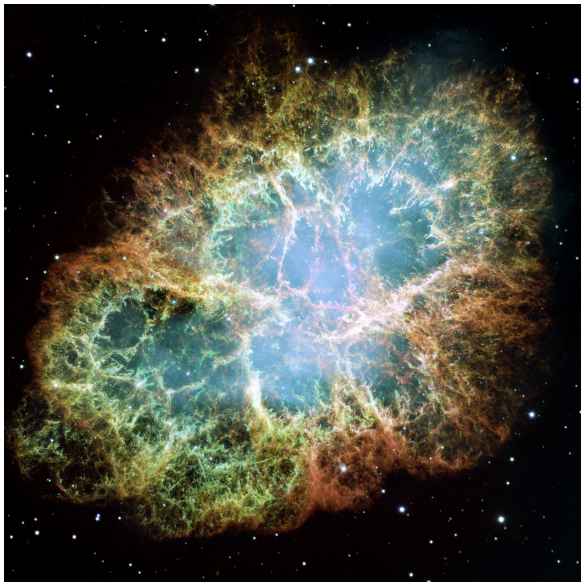

Figure 1.6: Image of the Crab Nebula, a supernova explosion remnant, by the Hubble Space Telescope. The explosion remnant is approximately six light years wide. Photo credit: National Aeronautics and Space Administration.

1.4 Thesis overview

As explained in this introduction, understanding mixing in compressible multiphase flows is important to many scientific and engineering problems. While experiments of these flows provide valuable insight into the flow dynamics, experiments are costly to design, manufacture, and implement. Additionally, because of the complex nature of the problems, the short time scales, and the multiphysics aspects of the

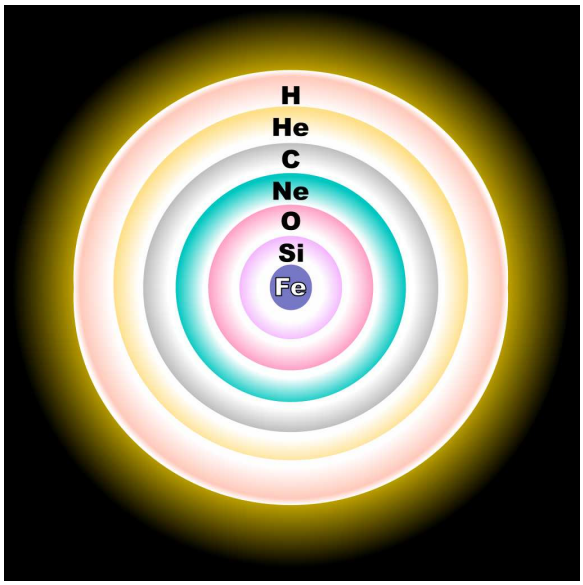

Figure 1.7: Illustration of the element shells of an evolved star before the supernova explosion. When the iron core becomes too massive, pressures in the core do not counterbalance gravitational forces and the core collapses, leading to a supernova explosion. Photo credit: wiki media.

flows, diagnostic tools can only offer limited information about the flow dynamics. The sensitivity of these flows to the initial conditions and material properties make it difficult to attain good repeatability.

Numerical simulations can circumvent these challenges and are a cost effective way of understanding the flow dynamics by exploring the relevant parameter space, isolating the physical effects of interest, and providing a complete description of the system's evolution. However, compressible multiphase flows are challenging to simulate as they require a robust and accurate treatment of flow discontinuities, which separate regions of different density, pressure, and velocity, high numerical resolution to resolve the disparate length and time scales, and methods adapted to unsteady flows. Numerical simulations of these flows are currently limited by (i) the numerical methods used to solve the partial differential equations describing the system, and (ii) the computational expense. In the first part of this thesis, we focus on addressing these two points. In the second part of the thesis, we use our computational framework to analyze several flow configurations of interest. This thesis has two main objectives:

1. We seek to develop an accurate and consistent numerical framework to simulate compressible multiphase flows. Our hypothesis is that the high-order Discontinuous Galerkin method, a powerful numerical method for discretizing flow evolution equations, must be adapted and combined with a suitable high performance computing paradigm to provide accurate physical insights into multiphase flow dynamics. Applying traditional numerical methods to the evolution equations describing compressible multiphase flows with interfaces can lead to spurious

numerical errors that change the dynamics of the flow, Section 2.1. These errors can result in an incomplete or erroneous understanding of the flow. The high computational resolution required to simulate the system accurately and the wide parameter space drives us to use graphics processing units, a novel parallel paradigm for high performance computing, Section 2.1. Finally, we provide improvements to the Discontinuous Galerkin method for the discretization of the advection term, Section 2.2.

2. Using this framework we explore the fundamental dynamics of compressible multiphase flows through the study of multilayered Richtmyer-Meshkov instabilities, Section 3.1, experiments of high-explosive driven Rayleigh-Taylor instabilities to understand beryllium strength, Section 3.2, supersonic deformation of droplets, Section 3.3, and blast-wave driven instabilities, Section 3.4. Our hypothesis is that the mixing dynamics in these flows can be controlled by appropriately changing the waves driving the instabilities and the material properties and configurations. We suggest that time-varying acceleration fields at interfaces and vorticity deposition dynamics can be used equivalently to describe perturbation growth evolution.

This work's main contributions to the field of numerical simulations of mixing in compressible multiphase flows are

- a new numerical method to simulate multiphase flows with different types of equations of state while avoiding spurious numerical errors that could contaminate the flow physics;

- a novel way of increasing the order of accuracy of the Discontinuous Galerkin method for the discretization of the advection term in evolution equations;

- a study of the multilayered Richtmyer-Meshkov instability, of particular applicability to inertial confinement fusion, illustrating control of the instability growth by tuning the material layers;

- a numerical analysis of experimental Rayleigh-Taylor instabilities in beryllium to validate material strength models;

- a new analytical model of different configurations of the blast-driven hydrodynamic instability.

CHAPTER II

Numerical Methods and Modeling for Shock Waves and Interfaces

In this chapter, we develop a numerical framework to simulate compressible multiphase flows. In Section 2.1, we discuss a novel numerical discretization which avoids spurious pressure oscillations. In Section 2.2, we provide improvements to the Discontinuous Galerkin method for the discretization of the advection term

2.1 *Past work*: A new limiting procedure for Discontinuous Galerkin methods applied to compressible multiphase flows with shocks and interfaces

This section presents the abstract, key figures, and conclusions of Henry de Frahan, M. T., Varadan, S. & Johnsen, E. 2015 A new limiting procedure for Discontinuous Galerkin methods applied to compressible multiphase flows with shocks and interfaces. *J. Comput. Phys.*, **280 (0)**, 489–509.

2.1.1 Abstract

Although the Discontinuous Galerkin (DG) method has seen widespread use for compressible flow problems in a single fluid with constant material properties, it has yet to be implemented in a consistent fashion for compressible multiphase flows with shocks and interfaces. Specifically, it is challenging to design a scheme that meets the following requirements: conservation, high-order accuracy in smooth regions and non-oscillatory behavior at discontinuities (in particular, material interfaces). Following the interface-capturing approach of Abgrall [43], we model flows of multiple fluid components or phases using a single equation of state with variable material properties; discontinuities in these properties correspond to interfaces. To represent compressible phenomena in solids, liquids, and gases, we present our analysis for equations of state belonging to the Mie-Grüneisen family. Within the DG framework, we propose a conservative, high-order accurate, and non-oscillatory limiting procedure, verified with simple multifluid and multiphase problems. We show analytically that two key elements are required to prevent spurious pressure oscillations at interfaces and maintain

conservation: (i) the transport equation(s) describing the material properties must be solved in a non-conservative weak form, and (ii) the suitable variables must be limited (density, momentum, pressure, and appropriate properties entering the equation of state), coupled with a consistent reconstruction of the energy. Further, we introduce a physics-based discontinuity sensor to apply limiting in a solution-adaptive fashion. We verify this approach with one- and two-dimensional problems with shocks and interfaces, including high pressure and density ratios, for fluids obeying different equations of state to illustrate the robustness and versatility of the method. The algorithm is implemented on parallel graphics processing units (GPU) to achieve high speedup.

2.1.2 Main result: elimination of spurious pressure oscillations in multiphase flows

Fig. 2.1 shows the pressure field at $t = 2$ (after one period) for the three numerical approaches:

A. Conservative transport equation for ρY as in [44], and limiting of the conserved variables $(\rho, \rho u, E, \rho Y)$, which we call the "fully conservative approach,"

B. Non-conservative transport equation for $1/(\gamma - 1)$ and limiting of the conserved variables $(\rho, \rho u, E)$ and $1/(\gamma - 1)$,

C. Non-conservative transport equation for $1/(\gamma - 1)$ and limiting of the variables $(\rho, \rho u, p, 1/(\gamma - 1))$, which we call "our approach."

The L_∞ error in the cell averages for pressure is $\mathcal{O}(10^{-2})$ with the fully conservative approach (A); it is smaller for approach B ($\mathcal{O}(10^{-3})$). For the proposed approach (C), it is essentially negligible ($\mathcal{O}(10^{-11})$). The pointwise errors are approximately two orders of magnitude larger. The errors for the first two approaches are observed to propagate away from the interface and affect the solution in the entire domain. The amplitude of these oscillations may grow physically upon interaction with other flow features. While these oscillations are small in this test case, we show in later validation tests that they propagate in the flow field, interact with other flow features, and cause the simulations to fail. It is clear that the errors arise for two reasons: the form of the transport equation for the material properties and the limiting procedure. The non-conservative formulation coupled with our modified limiting (our approach C) presents an oscillation-free pressure.

2.1.3 Conclusions

In this article, we introduce a solution-adaptive Discontinuous Galerkin method to simulate compressible multiphase flows with shocks and interfaces in a stable and accurate fashion. Following the interface-capturing approach of Abgrall [43], we model flows of multiple fluid components or phases using a single equation of state with varying material properties. To represent compressible phenomena in solids, liquids and gases, we consider the Mie-Grüneisen family of equations of state, which describes

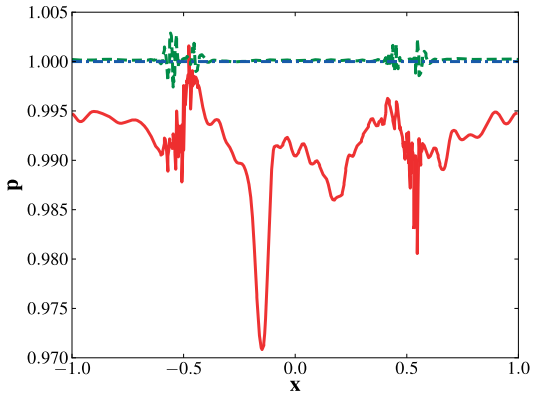

Figure 2.1: Pressure profile at $t = 2$ for the advection of a sharp material interface ($P = 2$, $\Delta x = 1/128$). Solid red: conservative transport equation and limiting of the conserved variables (fully conservative approach). Dashed green: non-conservative equation and limiting of the conserved variables. Dash-dotted blue: non-conservative equation and modified limiting (our approach).

a wide range of media, including stiffened and ideal gas equations of state. We show why spurious pressure oscillations occur in the DG framework when material properties vary, and how to remedy this problem. Using stringent test problems in one and two dimensions, we verify our approach. We can make the following conclusions:

- We develop a DG method that is conservative, non-oscillatory at interfaces (and shocks) and high-order accurate in smooth regions.
- Two key steps must be followed to avoid spurious pressure oscillations at interfaces between fluids of different material properties:
  1. Transport equations for appropriate material properties must be solved in a suitable weak form. *E.g*, for ideal gases, a non-conservative equation for $1/(\gamma - 1)$ must be solved, as suggested by Abgrall [43] for FV methods.
  2. Solution limiting must be applied to the appropriate variables (density, momentum, pressure, and the appropriate properties in the equation of state) to result in a non-oscillatory, conservative, and high-order accurate procedure. Limiting of the primitive variables does not ensure conservation. Our proposed approach does not require more operations than fully conservative limiting.
- We develop a new characteristic-based discontinuity sensor inspired by the physics for shocks, interfaces, and contacts.
- We can handle strong shocks in multi-dimensional settings involving possibly large density ratios for gas/gas, gas/liquid and fluid/solid interfaces in which the media obey an equation of state in the Mie-Grüneisen family.

- Results indicate that the largest errors are produced when solving the transport equation in conservative form and limiting the conserved variables (approach A). This approach fails for relatively simple problems involving gas/gas interfaces. Using a non-conservative transport equation and limiting the conserved variables (approach B) produces non-negligible errors shown to affect interface morphology in gas/gas problems and produce negative pressures in gas/liquid problems.

This work sets the basis for subsequent multiphysics research with DG using GPUs. We are also exploring potential inconsistencies with temperature fields for the compressible Navier-Stokes equations [45].

2.2 *Current work*: Accuracy Improvements for the Discretization of the Advection Term with the Discontinuous Galerkin Method

This section presents current work on improving the accuracy of the discretization of the advection terms by the Discontinuous Galerkin method. Some of the results and excerpts in this section have been published in Henry de Frahan, M. T., Khieu, L. & Johnsen, E. 2015 High-order Discontinuous Galerkin Methods Applied to Multiphase Flows. 22^d *AIAA Computational Fluid Dynamics Conference*, doi: 10.2514/6.2015-3045. We conclude this section with several thoughts for successfully completing the project.

2.2.1 Introduction

The Discontinuous Galerkin (DG) method is a numerical method for partial differential equations in which the solution is discretized in a computational cell through an expansion in terms of polynomial basis functions. This approach combines advantages of the finite element and the finite volume (FV) methods. In addition to being high-order accurate, the DG method is a compact-stencil scheme, so it is highly scalable on parallel architectures, and implementable on unstructured grids. The discontinuity in basis functions representing the solution naturally provides a means to introduce dissipation where needed. As with the FV methods, physical fluxes between neighboring cells are calculated using Riemann solvers. The DG approach exhibits superconvergence properties for the advection terms, at a rate of $2p+1$, where p is the polynomial order [46, 47]. Cockburn and Shu popularized the Runge-Kutta Discontinuous Galerkin (RKDG) for time-dependent convection-dominated problems [48, 49, 50, 51, 52]. Shocks and discontinuities can accurately be captured using limiters to dampen the oscillations that are caused by high-order interpolation across a discontinuity [49, 53, 54, 55, 56, 57, 58].

Because of the discontinuous representation of the solution at the cell interfaces, the DG method is not naturally amenable to discretizing second order derivatives, which appear, for example, in the diffusion terms of the Navier-Stokes equations. Past approaches to resolving this issue have involved interior penalty methods for

elliptic and parabolic equations [59, 60, 61] and rewriting the second order terms as a system of first order derivatives [62, 63]. The drawback is that there is no consistent approach and the methods require tunable parameters. The Recovery Discontinuous Galerkin (RDG) method was developed to provide a unified and consistent framework for discretizing second order derivatives [64, 65, 66]. The method removes the discontinuity at the interface by recovering the underlying high-order polynomial spanning neighboring cells. This is done by matching polynomial moments in cells that share interfaces. The RDG method is stable, works in multiple dimensions, and can be applied to non-linear diffusion operators. It also exhibits superconvergent properties at a rate of $3p+2$. However, using the RDG method leads to a mismatch in the convergence properties of the advection terms $(2p+1)$ and the diffusion terms $(3p+2)$. In a system containing both advective and diffusive processes, the numerical discretization of the diffusive terms is more accurate than that commonly used for the advective terms of the partial differential equations. This mismatch in the order of accuracy implies that the convergence of a simulation with advective and diffusive processes will be dominated by the slower advective convergence rate. Improving the order of accuracy of the discretization of the advection terms would allow us to converge equally rapidly for both the diffusive and advective processes. This is important when simulating large systems requiring high numerical resolution, such as direct numerical simulations of turbulent processes.

The present paper builds on previous research [67] to fix the order of accuracy mismatch between the advection and diffusion discretizations by increasing the discretization order of accuracy of the advection terms.

2.2.2 Preliminary Work

Systematic approaches to exploring improvements to the DG scheme have previously been presented [67]. This previous work has shown that an improved DG scheme for advection called interface-centered reconstruction with binary projection, denoted ICB, exhibits a $3p+1$ order of accuracy and has reasonable stability properties. We recall the scheme here and study its stability properties.

We consider, without loss of generality, the one-dimensional hyperbolic equation

$$\frac{\partial u}{\partial t} + \frac{\partial F}{\partial x} = 0 \tag{2.1}$$

for the conserved variable u, where $F(t,x,u)$ is the flux. In the DG scheme, the solution u is expanded in each cell of the domain Ω_j in terms of $p+1$ basis functions $\phi_n(x)$, $u_j(t,x) \approx u_h(t,x) = \sum_{n=0}^{p} u_n(t)\phi_n(x)$. The flux at an arbitrary interface $j+1/2$ is evaluated using a Riemann solver, which involves the left and right values of u at that interface, u_L and u_R, which are provided by the polynomial representation of u_j and u_{j+1}. The cells $j-1$, j, and $j+1$ represent the computational stencil of the DG method used to evolve the solution in time. This compact stencil is one of the method's defining properties and we wish to keep the stencil compact when improving the DG method. Improvements to the basic DG advection scheme rely on increasing the polynomial order of the numerical representations u_j and u_{j+1} to

calculate $\hat{u}_{j+1/2,L}(x)$ and $\hat{u}_{j+1/2,R}(x)$, from which u_L and u_R are evaluated.

The central idea of the ICB scheme is as follows. The reconstruction of $\hat{u}_{j+1/2,L}(x)$ is biased towards the left, cell j, meaning that the enhanced representation can contain more moments of u_j than u_{j+1},

$$\int_{x_{j-1/2}}^{x_{j+1/2}} \phi_n^j \hat{u}_{j+1/2,L}\,\mathrm{d}x = \int_{x_{j-1/2}}^{x_{j+1/2}} \phi_n^j u_j\,\mathrm{d}x \qquad n = 0,\ldots,p \tag{2.2a}$$

$$\int_{x_{j+1/2}}^{x_{j+3/2}} \phi_n^{j+1} \hat{u}_{j+1/2,L}\,\mathrm{d}x = \int_{x_{j+1/2}}^{x_{j+3/2}} \phi_n^{j+1} u_{j+1}\,\mathrm{d}x \qquad n \in \mathcal{N} \tag{2.2b}$$

where $\mathcal{N}$ is a subset of $\{0,\ldots,p\}$, the set of indexes of the moments of the original polynomial. A similar set of equations can be derived for $\hat{u}_{j+1/2,R}(x)$, which is then biased towards cell $j+1$. This binary reconstruction scheme achieves a $3p+1$ order of accuracy if $\mathcal{N}$ contains p original moments. This implies that there are $p+1$ subsets $\mathcal{N}$ formed with combinations of the set $\{0,1,\ldots,p\}$, leading to $p+1$ reconstructions schemes that exhibit $3p+1$ accuracy. We denote the schemes of this type by `icb`#1[#2] where #1 is the original polynomial order p and #2 is the subset $\mathcal{N}$.

2.2.2.1 Von Neumann Stability Analysis

To study the stability of our DG enhancement scheme, we analyze the scalar linear advection equation 2.1, where $F(t,x,u) = au$ and $a > 0$. The DG update equations are:

$$\frac{\mathrm{d}}{\mathrm{d}t}\int_{\Omega_j} v_j u_j\,\mathrm{d}x = -a\int_{\Omega_j} v_j \frac{\partial u_j}{\partial x}\,\mathrm{d}x,$$

and, using integration by parts,

$$\frac{\mathrm{d}}{\mathrm{d}t}\int_{\Omega_j} v_j u_j\,\mathrm{d}x = -a[v_j u_j]_{x_{j-1/2}}^{x_{j+1/2}} + a\int_{\Omega_j} \frac{\partial v_j}{\partial x} u_j\,\mathrm{d}x,$$

where v_j is a test function in Ω_j. By using the solution basis functions as the test functions, expanding $u(t,x)$ on the solution basis, and using an upwind flux (without loss of generality), we rewrite the update equations as a linear system for the solution coefficients:

$$\frac{\Delta x}{a}\frac{\mathrm{d}}{\mathrm{d}t}\mathbf{u}_j = \mathbf{M}(T)\mathbf{u}_j$$

where T represents the translation of the solution by one cell: $T\mathbf{u}_j = \mathbf{u}_{j+1}$ and $T^{-1}\mathbf{u}_j = \mathbf{u}_{j-1}$. The Fourier transform of $\mathbf{M}(T)$, $\widehat{\mathbf{M}}(\beta)$, is obtained by subsituting T for its transform $e^{i\beta}$. Calculations of the eigenvalues of $\widehat{\mathbf{M}}(\beta)$ and their respective Taylor-series expansions are used to compare with the exact differential operator, $\lambda_e = -i\beta$, and establish the stability and order of accuracy of the numerical scheme.

For $p = 1$, we can construct two enhancement schemes, `icb1`[0] and `icb1`[0], to

enhance the cell interface values. Von Neumann analysis of the resulting schemes show that both schemes are stable ($\Re(\lambda_i) \leq 0 \; \forall \; i = 0, \ldots, p$), Figure 2.4, and exhibit fourth order accuracy.

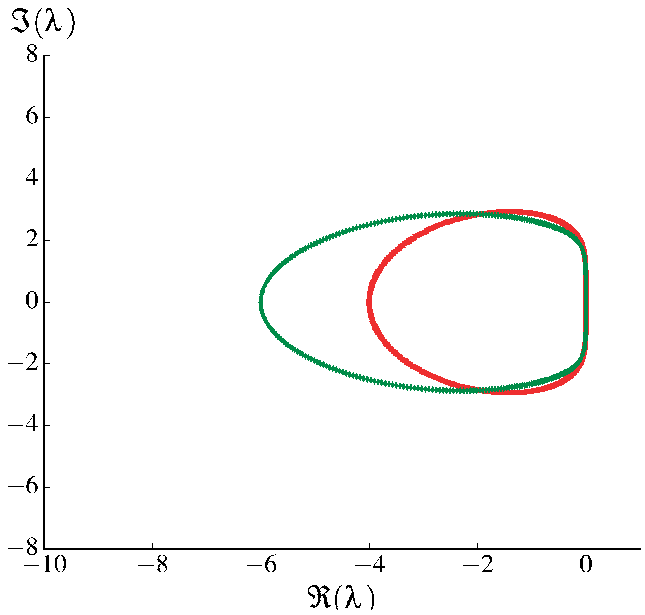

Figure 2.2: Loci of eigenvalues of the enhanced schemes for $p = 1$ in the complex plane. Red squares: `icb1`[0]; green diamonds: `icb1`[0].

For $p = 2$, there are three optimal enhancement schemes, `icb2`$[0, 1]$, `icb2`$[1, 2]$, and `icb2`$[0, 2]$. These schemes lead to seventh order accuracy (as opposed to fifth order accuracy for standard DG). However, as illustrated in Figure 2.3b, the real part of the eigenvalues are positive for some values of β. This incursion into the real positive half of the complex plane can lead to numerical instabilities if the time-marching scheme is inadequate. These incursions are small enough (their maximum value is 0.00073) to be covered by a standard Runge-Kutta 4 time integration scheme. However, this implies the existence of a lower bound on the CFL number to ensure that the scheme remains stable. For very small CFL numbers, these incursions will eventually lie outside the region of stability of the time-integration scheme.

For $p = 2$, instead of using two moments from neighboring cells to enhance the interface, we can use suboptimal sets consisting of using only one moment of the neighboring cell: `icb2`[0], `icb2`[1], and `icb2`[2]. These suboptimal schemes are stable and exhibit sixth order accuracy.

In conclusion, Von Neumann analysis of our enhancement method shows that, for the one-dimensional scalar advection equation and for various suboptimal choices of the set $\mathcal{N}$, the scheme exhibits improved convergence and is stable. Using one moment from the neighboring cell for the enhancement scheme leads to a stable and $2p + 2$ order of accuracy scheme. Including additional moments in the enhancement scheme leads to a numerical method with increased accuracy but unstable properties. We propose to address the stability issues in the coming months by following the ideas in Section 2.2.3.

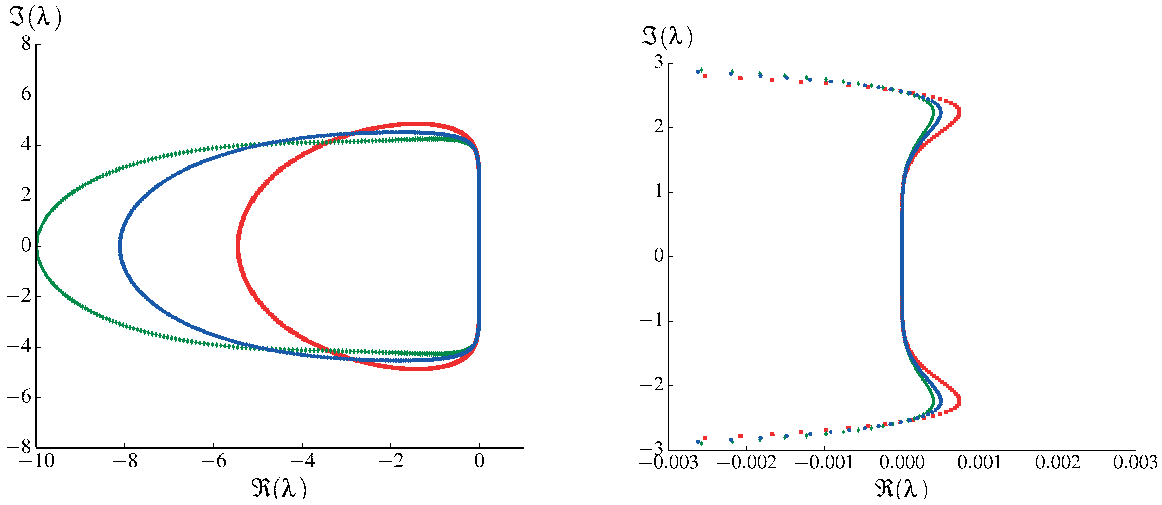

(a) Eigenvalue loci.

(b) Zoom of Figure 2.3a.

Figure 2.3: Loci of eigenvalues of the enhanced schemes for $p = 2$ in the complex plane. Red squares: `icb2`$[0, 1]$; green diamonds: `icb2`$[1, 2]$; blue circles: `icb2`$[1, 2]$.

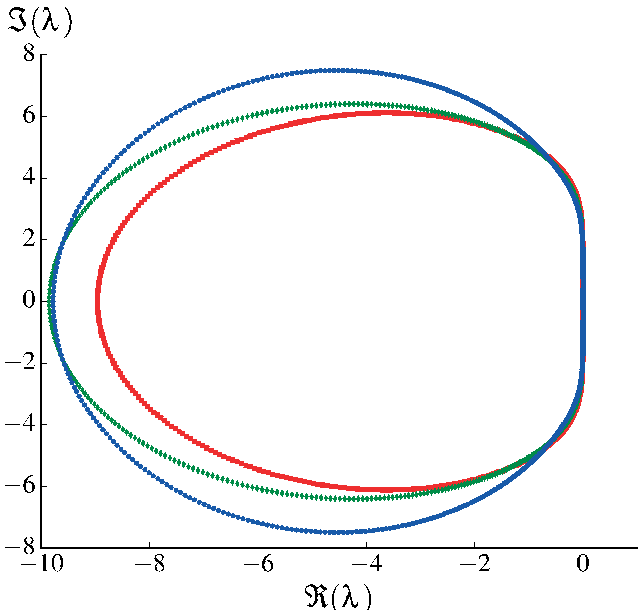

Figure 2.4: Loci of eigenvalues of the enhanced schemes for $p = 2$ in the complex plane. Red squares: `icb2`$[0]$; green diamonds: `icb2`$[1]$; blue circles: `icb2`$[2]$.

2.2.3 Proposed work

We are currently exploring different numerical schemes to either stabilize the `icb` schemes or develop different schemes which will increase the order of accuracy of the DG method, including:

- developing a stable linear combination of different order `icb` schemes combining different neighboring moments;
- implementing a hierarchical reconstruction procedure using `icb` schemes of lower moments to reconstruct higher order moments;
- using different basis functions for the enhanced polynomial interpolations.

CHAPTER III

Numerical Investigation of Interface Evolution Following the Passage of a Shock Wave

This chapter focuses on physical discussions of shocks interacting with interfaces in compressible multiphase flows. We discuss the multilayered Richtmyer-Meshkov instabilities, Section 3.1, experiments of high-explosive driven Rayleigh-Taylor instabilities to understand beryllium strength, Section 3.2, supersonic deformation of droplets, Section 3.3, and blast-wave driven instabilities, Section 3.4.

3.1 *Past work*: Numerical simulations of a shock interacting with successive interfaces using the Discontinuous Galerkin method: the multilayered Richtmyer-Meshkov and Rayleigh-Taylor instabilities

This section presents the abstract, key figures, and conclusions of Henry de Frahan, M. T., Movahed, P. & Johnsen, E. 2015 Numerical simulations of a shock interacting with successive interfaces using the Discontinuous Galerkin method: the multilayered Richtmyer–Meshkov and Rayleigh–Taylor instabilities. *Shock Waves*, **25 (4)**, 329–345.

3.1.1 Abstract

In this work, we investigate the growth of interface perturbations following the interaction of a shock wave with successive layers of fluids. Using the Discontinuous Galerkin method, we solve the two-dimensional multifluid Euler equations. In our setup, a shock impacts up to four adjacent fluids with perturbed interfaces, Figure 3.1. At each interface, the incoming shock generates reflected and transmitted shocks and rarefactions, which further interact with the interfaces. By monitoring perturbation growth, we characterize the influence these instabilities have on each other and the fluid mixing as a function of time in different configurations. If the third gas is lighter than the second, the reflected rarefaction at the second interface amplifies the growth at the first interface. If the third gas is heavier, the reflected shock decreases the growth and tends to reverse the Richtmyer–Meshkov instability as the thickness of

the second gas is increased. We further investigate the effect of the reflected waves on the dynamics of the small scales and show how a phase difference between the perturbations or an additional fluid layer can enhance growth. This study supports the idea that shocks and rarefactions can be used to control the instability growth.

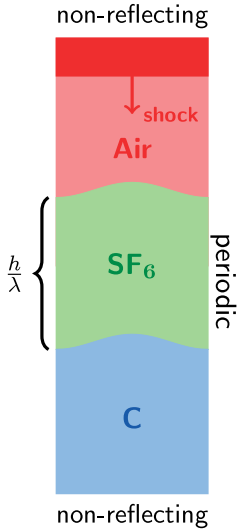

Figure 3.1: Baseline multi-layered problem setup.

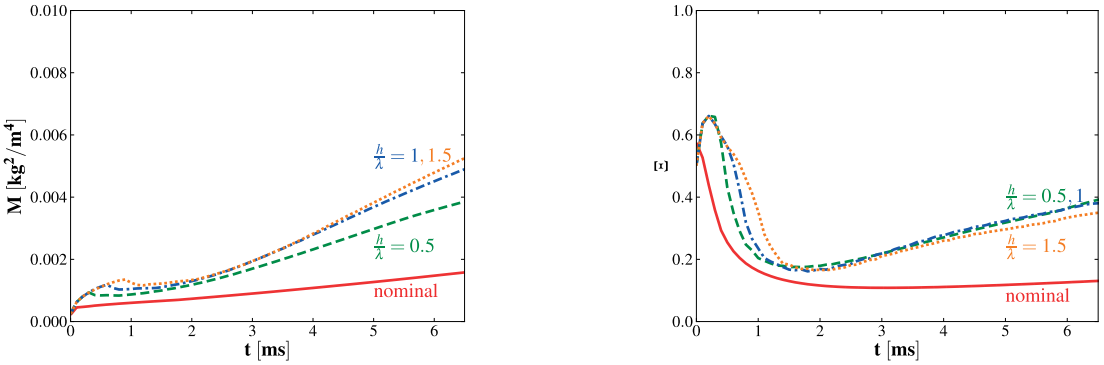

(a) M. (b) Ξ.

Figure 3.2: Mixing metrics versus time for the baseline problem with a light third gas for different thicknesses of SF_6 (middle gas).

3.1.2 Conclusions

In this work, we used a high-order accurate Discontinuous Galerkin method to simulate the interaction of a shock wave with successive interfaces separating different gases. In particular, we investigated the effect of the acoustic impedance (and density) of the third gas on the growth of the RMI at the different interfaces. Through this study, we make the following conclusions:

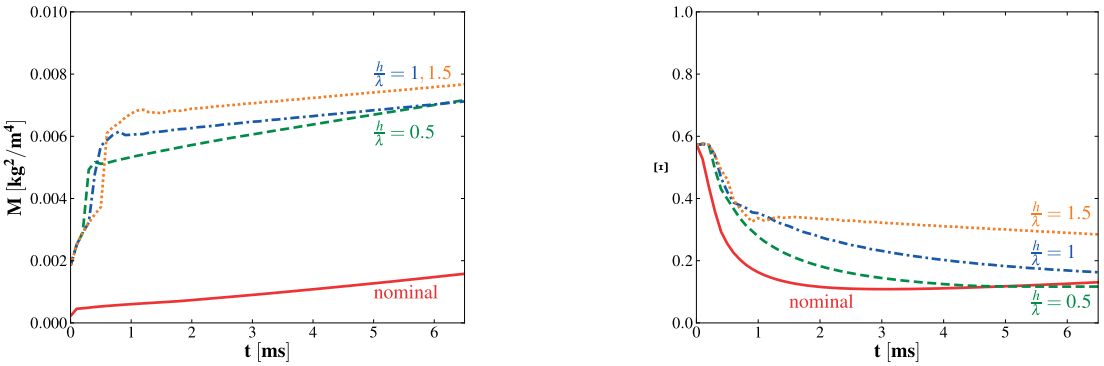

(a) M. (b) Ξ.

Figure 3.3: Mixing metrics versus time for the baseline problem with a heavy third gas for different thicknesses of SF_6 (middle gas).

- If the third gas is lighter than the second gas, the reflected rarefaction at the second interface amplifies the growth at the first interface for two main reasons: the reflected rarefaction deposits vorticity in the same direction as the incoming shock and the perturbation amplitude at the time of interaction with the rarefaction has grown. If the third gas is heavier, the reflected shock decreases the growth and tend to reverse the perturbation growth as the thickness of the second gas increases. This behavior is governed by Richtmyer–Meshkov (instantaneous acceleration of the interface) and Rayleigh–Taylor (acceleration of a heavy fluid into a light one) instabilities, which are both transient in this problem.

- The results strongly depend on the separation distance between the interfaces. We observed freeze-out in the case of a heavy third gas. This study supports the idea that perturbation growth may be controlled using rarefactions and shocks [35].

- We characterized fluid mixing through two different metrics. The light third gas resulted in higher fluid mixing (Figure 3.2) relative to entrained unmixed fluid than the heavy third gas case (Figure 3.3).

- To represent the behavior at the small scales, we characterized the temporal evolution of enstrophy and energy of the small scales by relating this to the effect of the reflected waves.

- The phase difference between the perturbations does not affect the growth if the interfaces are far from each other. Because of baroclinic vorticity and interface proximity, the phase difference has a significant effect on the growth if the interfaces are initially close to each other.

- By adding a fourth gas, we can significantly increase the growth in a light-heavy-light-heavy or a light-heavy-heavier-light configuration. This effect is due to the

RT-unstable phase of the growth induced by reflected rarefactions.

The present work presents an exploration of a small range of the parameter space; future exploration of the number of layers, gas properties and thicknesses, and amplitude properties are desirable to better understand this problem. This study forms the basis for further three-dimensional studies of randomly perturbed interfaces, transition to turbulence, and late-time mixing evolution. A more in-depth investigation of such a set-up may be beneficial to control perturbation growth in ICF.

3.2 *Past work*: Experimental and numerical investigations of beryllium strength models using the Rayleigh-Taylor instability

This section presents the abstract, key figures, and conclusions of Henry de Frahan, M. T., Belof, J. L., Cavallo, R. M., Raevsky, V. A., Ignatova, O. N., Lebedev, A., Ancheta, D. S., El-dasher, B. S., Florando, J. N., Gallegos, G. F., Johnsen, E. & LeBlanc, M. M.. 2015 Experimental and numerical investigations of beryllium strength models using the Rayleigh-Taylor instability *J. Appl. Phys.*, **117 (22)**, 225901.

This work was featured on the cover of volume 117 (issue 22) of the Journal of Applied Physics and was the subject of a Lawrence Livermore National Laboratory news article [68].

3.2.1 Abstract

We present a set of high explosive driven Rayleigh-Taylor strength experiments for beryllium to produce data to distinguish predictions by various strength models. Design simulations using existing strength model parameterizations from Steinberg-Lund and Preston-Tonks-Wallace (PTW) suggested an optimal design that would delineate between not just different strength models, but different parameters sets of the PTW model. Application of the models to the post-shot results, however, suggests growth consistent with little material strength, Figure 3.5. We focus mostly on efforts to simulate the data using published strength models as well as the more recent RING relaxation model developed at VNIIEF. The results of the strength experiments indicate weak influence of strength in mitigating the growth with the RING model coming closest to predicting the material behavior. Finally, we present shock and ramp-loading recovery experiments.

3.2.2 Discussion and Conclusion

We performed six HE-driven Be RT experiments to discriminate among different strength models, Figure 3.4. These experiments were designed to reach a phase space where the models' growth predictions differed, Figure 3.6. Relative to the predicted behavior, the data suggest that the Be ripples growth was only slightly mitigated by strength, indicating weaker than anticipated strength, Figure 3.5. The RING model

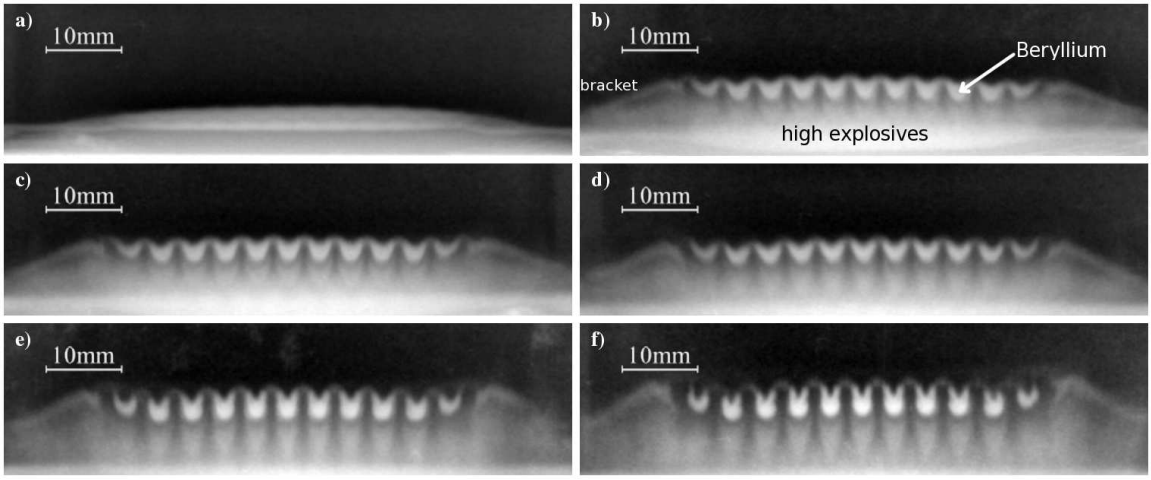

Figure 3.4: Radiographs of the six HE driven Be RT experiments. The brighter area on the bottom of the radiograph is the HE. The clear white region in the center of the radiograph is the Be liner. (a) $A_0 = 0.38$mm, $h = 1.78$mm, $S = 1.4 \pm 0.2$mm, $A = 0.6 \pm 0.1$mm; (b) $A_0 = 0.48$mm, $h = 2$mm, $S = 6.3 \pm 0.3$mm, $A = 2.4 \pm 0.1$mm; (c) $A_0 = 0.48$mm, $h = 2$mm, $S = 7.1 \pm 0.3$mm, $A = 2.6 \pm 0.1$mm; (d) $A_0 = 0.38$mm, $h = 1.78$mm, $S = 8.9 \pm 0.3$mm, $A = 2.7 \pm 0.2$mm; (e) $A_0 = 0.48$mm, $h = 2$mm, $S = 11.7 \pm 0.3$mm, $A = 3.6 \pm 0.2$mm; (f) $A_0 = 0.48$mm, $h = 2$mm, $S = 14.6 \pm 0.2$mm, $A = 4.1 \pm 0.2$mm. A_0 is the initial peak-to-valley perturbation amplitude, h is the initial target thickness, S is the target displacement, and A is the measured peak-to-valley perturbation amplitude. The direction of motion is towards the top of the images.

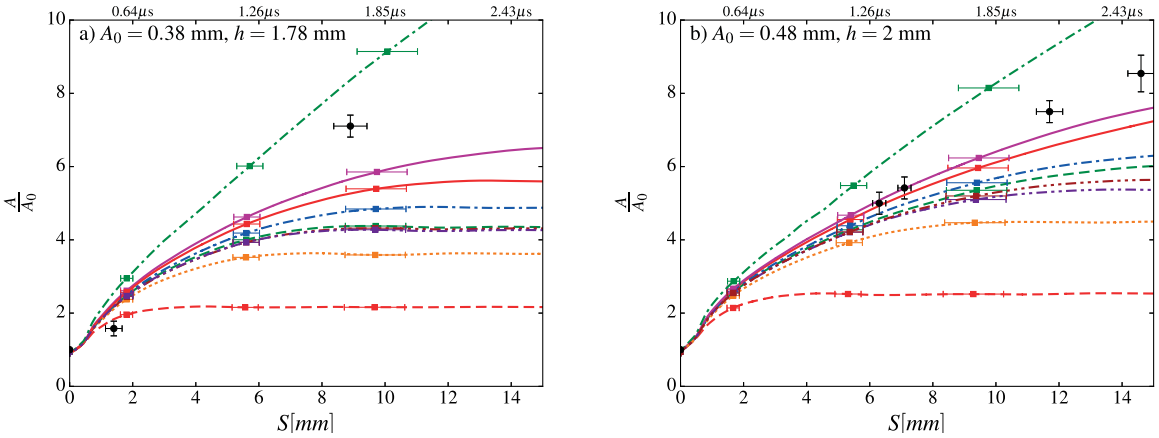

Figure 3.5: Growth factors as a function of displacement. Left (a): $A_0 = 0.38$mm and $h = 1.78$mm; right (b): $A_0 = 0.48$mm and $h = 2$mm. Black dots: experimental data; dotted-dashed green: no strength; solid red: SCG; dashed green: SL; dotted-dashed blue: PTW; dotted orange: PTW (Preston); dotted- dotted-dashed purple: PTW (Chen); dotted-dotted-dotted-dashed burgundy: PTW (Blumenthal); solid magenta: RING; dashed red: MTS. The error bars for the simulated growth factors are representative single point error bars capturing uncertainties in the simulated drive with respect to the scatter among the experimental drive measurements. These error bars were obtained by propagating the uncertainty in the simulated drives.

does reasonably well predicting the growth for the larger initial amplitude experiments. The other models under-predict the perturbation growth. The experimental results challenge the underlying assumptions of the existing strength models. Once the material enters a strain, strain-rate, and pressure phase space far from the calibration regimes of the current models, its predicted behavior breaks down. In part, the models rely on a limited range of data, but also limited physical assumptions, mostly having to do with how strain and strain rate carry the plastic flow. For example, the results raise questions about the ansatz formulations, such as what are the proper rate hardening relationships in the thermal activation and phone drag regimes; where do the regimes even cross; are strain and strain rate the proper independent variables or should they be explicitly replaced with dislocation density and velocity? To complicate the challenge of developing a complete constitutive model for Be, the recovery experiments showing a twinning fraction of slightly less than 50% suggest that twining should not be overlooked as an important physical mechanism in the material flow. Furthermore, while the RT experiments show no observable spall or cracks at length scales that could be imaged, the recovery experiments do. Granted, the loading profiles between the two experiments differ, and the recovery experiments by their nature are done late in time, long after release waves have traversed the samples. However, the recovery experiments do suggest failure mechanisms should be included in any advanced Be plasticity model. As such, experiments might be done that are specifically designed to catch material failure under loading to determine if the behavior observed in these experiments is more a result of failure mechanisms,

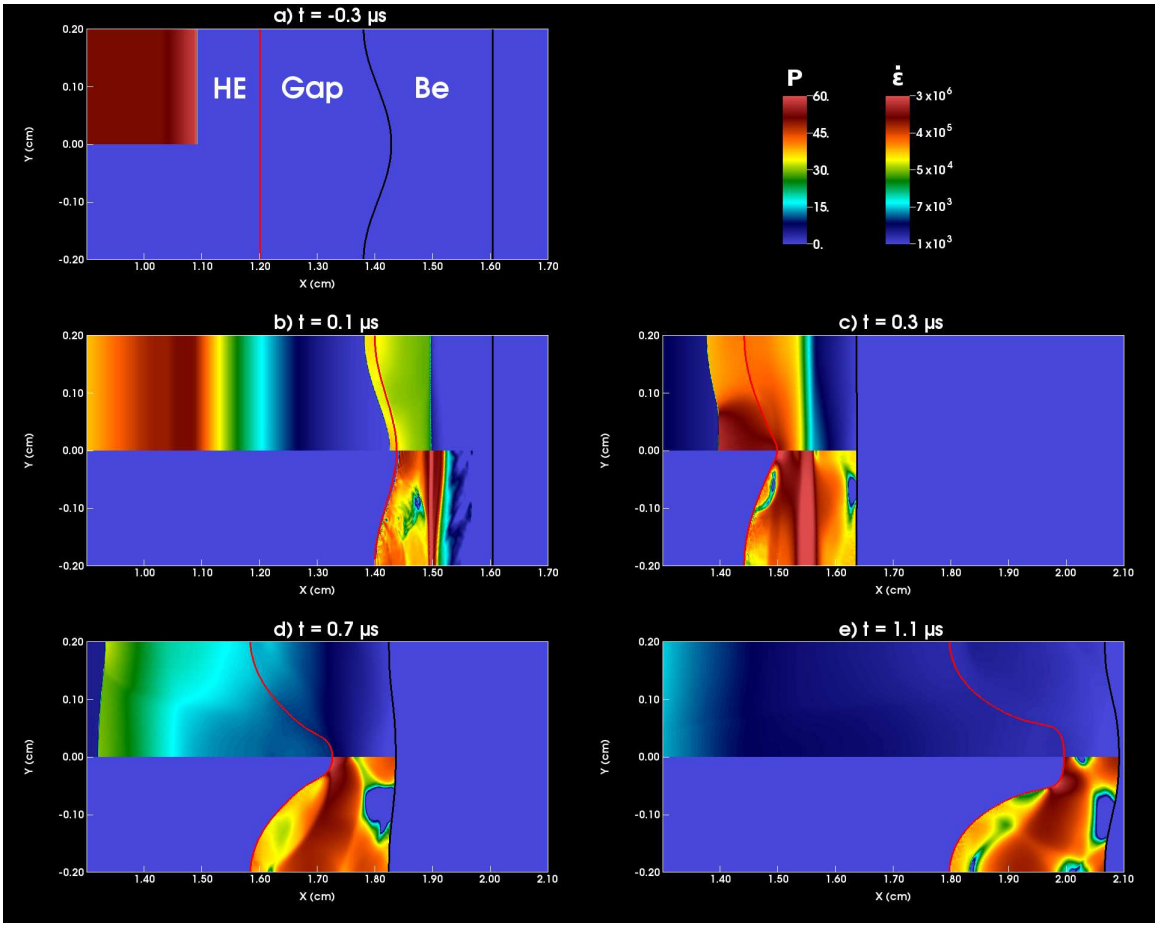

Figure 3.6: Pseudocolors of pressure (top half) and strain-rates (bottom half) in the HE and Be target. Red line: HE-Be interface; black line: Be back. $t = 0$ is the HE arrival time at the Be/HE interface. Pressure color map is in units of GPa with min=0 GPa and max=60 GPa. Strain-rate color map is in units of s^{-1} with min $= 10^3 s^{-1}$ and max $= 3 \times 10^6 s^{-1}$. (a) $t = -0.3\mu s$; (b) $t = 0.1\mu s$; (c) $t = 0.3\mu s$; (d) $t = 0.7\mu s$; (e) $t = 1.1\mu s$.

such as shear localization, or if indeed the plastic flow is truly a result of weaker constitutive properties than those predicted by most models.

If similar experiments are proposed for future work, we recommend adjusting the existing models to match the data set presented here and then driving the targets through different regions of stress-strain-rate phase space by adjusting drive or initial perturbations, or by tamping the target to maintain the Be at pressure for longer periods of time. Varying the initial perturbation wavelength would lead to a dispersion curve that could increase our understanding of Be strength in these extreme regimes while higher temperature experiments could also be a means to distinguish the models in future experiments.

3.3 *Past work*: Supersonic flow around a water droplet

This section presents parts of the abstract, key figures, and conclusions of Henry de Frahan, M. T., Khieu, L. & Johnsen, E. 2015 High-order Discontinuous Galerkin Methods Applied to Multiphase Flows. 22^d *AIAA Computational Fluid Dynamics Conference*, doi: 10.2514/6.2015-3045.

3.3.1 Abstract

We present numerical simulations of a multiphase problem applicable to many engineering fields, including fuel injection, plasma deposition, raindrops impacting high speed vehicles, and turbomachinery[25, 26]. Simulations of a shock interacting with a drop of water in air are compared to experimental data. We present the flow dynamics and discuss the interactions between a supersonic air flow and a compliant water cylinder.

3.3.2 Conclusions

Using the high-order DG method combined with a non-oscillatory reconstruction procedure, we simulated a multiphase problem of relevance to many engineering applications. In this problem, an initial 2D water drop is stationary in air. A Mach 2.5 shock coming from the left impinges on the drop, Figure 3.8. This setup is similar to past experiments and simulations of a shock interacting with a water column [70, 71]. As the shock impinges on the drop, it creates a supersonic flow around the drop. The initial shock is deflected by the drop and the reflected shock evolves into a bow shock. Baroclinic vorticity generated at the drop surface by the passage of the shock creates a wake downstream of the drop which forms into a reentrant flow at later times. This flow causes a decrease in the drop width and an increase in the height. The strong coupling between the wave dynamics and the deforming geometry causes a series of compressions which steepen into shocks in the wake of the drop. There is good qualitative agreement with the experiments as the shape and wake of the drop in both the simulation and experiment look similar. We also showed very good quantitative agreements between simulation results and past experiments [70].

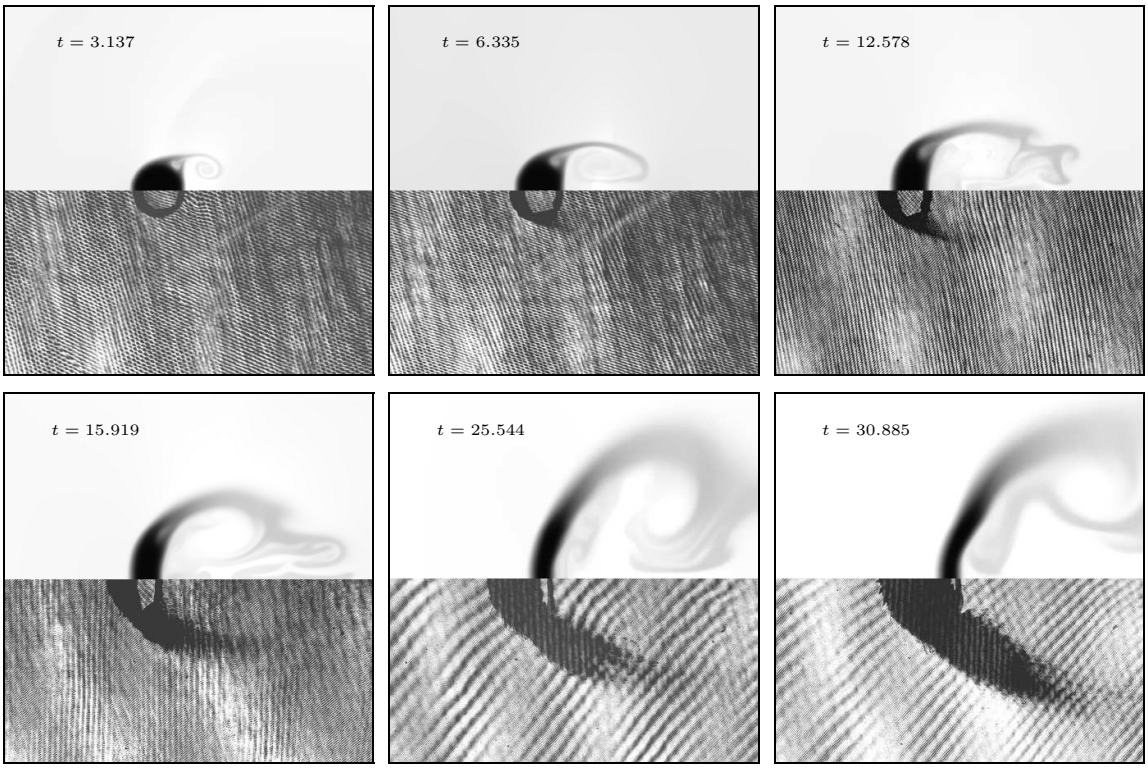

Figure 3.7: Comparison of experimental visualization of the droplet using a holographic interferogram [69, 70] (bottom) and simulated density (top) at a 1.18 Mach number.

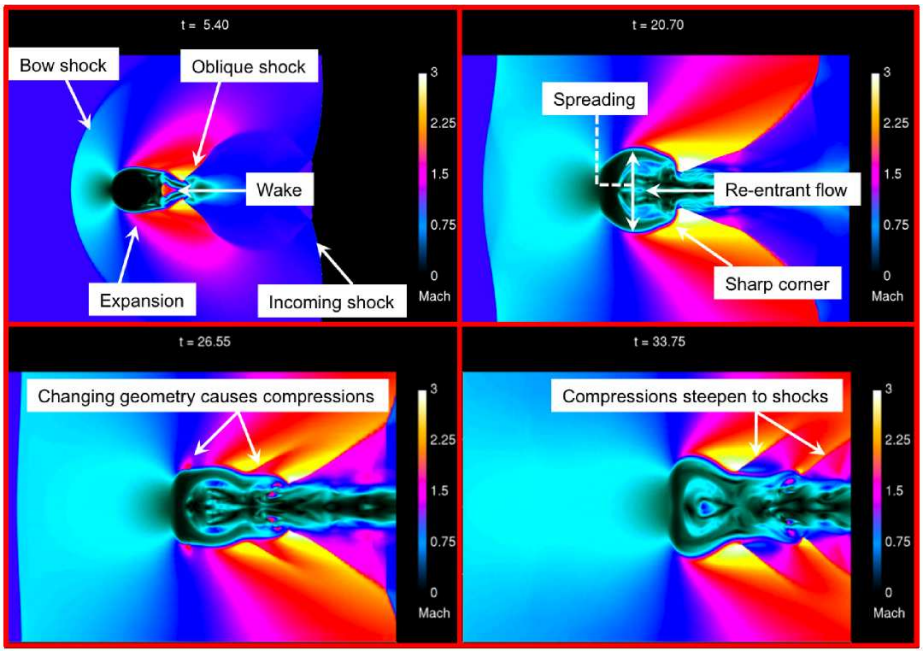

Figure 3.8: Mach contours of shock-droplet interaction (shock mach number = 2.5).

3.4 *Current work*: Blast-driven hydrodynamic instabilities

This section presents current work on studying blast-driven hydrodynamic instabilities. We introduce the topic through a literature review and propose some directions for successful completion of this project.

3.4.1 Introduction and literature review

Blast wave-driven hydrodynamic instabilities are prevalent in many different scientific and engineering applications [72, 35, 73, and references therein]. Blast waves are formed by a sudden localized deposition of energy which increases the density and pressure of the material at that point[74, 75]. This deposition of energy leads to a shock moving outwards from the energy source point and a rarefaction wave which follows behind the shock. The rarefaction eventually overtakes the shock and decreases its strength until the shock vanishes.

In astrophysics, the explosion from a supernova initiates a blast wave which interacts with many different layers of materials as it radiates outwards from the center of the core collapse [76, 77]. Collisions of comets with planets and their atmospheres may lead to blast waves interacting with different materials [78]. A solar flare can also form a blast wave which then interacts with the solar wind [38]. In inertial confinement fusion, the shape of the laser pulse used to heat the hohlraum walls and generate x-rays is designed to generate shocks to compress the deuterium and tritium fuel in the capsule. The first laser pulse is usually followed by a slight decrease in power, implying that the first shock is followed by a rarefaction, similarly to a blast wave.

As a blast wave interacts with a perturbed interface between two fluids, two important hydrodynamic instabilities take place [19]. The shock at the front of a blast wave initiates a Richtmyer-Meshkov instability [1] by instantaneously depositing baroclinic vorticity at the interface because of the misalignment of the pressure gradient across the shock and the density gradient across the interface. The rarefaction which immediately follows the shock front imposes a time varying acceleration of the interface, leading to the well-known Rayleigh-Taylor instability [79, 9].

While shock accelerated or Richtmyer-Meshkov instabilities and constant acceleration Rayleigh-Taylor instabilities have been extensively studied in the past [3, 80, 81], blast wave-driven hydrodynamic instabilities and hydrodynamic instabilities with time varying accelerations have recently generated some interest in the community.

Drake et al. [82] performed initial blast wave-driven experiments of a three-dimensional "egg-crate" patterned perturbation. The experiments suggested that the Rayleigh-Taylor spikes (dense material penetrating into a less dense one) overtook the shock. Kuranz et al. [19] studied the perturbation growth by considering both the compressibility effects of the blast wave as well as the Rayleigh-Taylor instability process due to the blast wave acceleration of the interface. Kuranz et al. [83] performed blast wave-driven instability experiments to study spike penetration. Experimental results showed narrow spikes penetrating deep behind the blast wave shock front. Discrepancies in spike penetration and morphology with simulations

were discussed and several hypotheses were explored.

Computational studies of blast-driven perturbations have explored the effect of the initial conditions on late-time mixing dynamics and transition to turbulence. Miles et al. [84] performed simulations of two-dimensional multimode blast-driven instabilities at drive conditions similar to those achievable at the National Ignition Facility. The authors did not find a self-similar behavior for the development of the mixing layer and showed sensitivity of the mixing layer width to the initial conditions. In a similar study, Miles et al. [18] simulated strong blast waves interacting with perturbed interfaces and discussed the effects of the spike-spike and bubble-bubble interaction on the mix layer growth. In [85], the flow's transition to turbulence was shown to be sensitive to the initial conditions and spectra of the perturbations. Miles [86] combines a buoyancy-drag and bubble-merger model with divergence and compressibility effects and compares the predictions to simulations of cylindrical blast wave-driven instabilities. Finally, [87] used simulations to study the effects of a blast wave interacting with a bubble on suppressing the vorticity production by the rarefaction.

Models for hydrodynamic instabilities generally follow two different directions: the first uses vorticity models to infer the perturbation growth, the second relies on potential flow models. Our discussion will focus on models that pertain to hydrodynamic instabilities driven by blast waves or subject to time varying accelerations.

Vortex models for the Richtmyer-Meshkov instability were first proposed by Samtaney and Zabusky [7], Zabusky et al. [88], Zabusky [89]. Jacobs and Sheeley [8] modeled the growth of single-mode Richtmyer-Meshkov instability experiments by assuming a row of line vortices at the interface. Similarly, Rikanati et al. [90] expanded this model and used multi-mode Richtmyer-Meshkov instabilities to validate a model of the mixing zone growth using vortex dynamics. Vortex deposition models have had much success modeling Richtmyer-Meshkov instabilities [91, 92, 93, 94, 95].

Using potential flow arguments, Oron et al. [17] proposed a buoyancy drag model for the late-time growth of bubbles subject to a Rayleigh-Taylor instability with time varying acceleration. Srebro et al. [96] expanded this model to span the early-mid-late time growth evolution by incorporating exponential decay terms based on the perturbation growth. Miles [97, 98] develop a buoyancy drag model for blast-driven instabilities which incorporate the effects of the shock (Richtmyer-Meshkov instability), compressibility, and time dependent acceleration (Rayleigh-Taylor instability). This model was compared successfully to experiments by Kuranz et al. [19]. Miles [97] presents a bubble merger model for multimode perturbations interacting with blast waves. Building on [99], Mikaelian [100] proposed a generalized Layzer model for non-constant complex accelerations of perturbed interfaces with time-varying Atwood numbers. This modeled resulted in a coupled set of ordinary differential equations to solve numerically. Drake [101] modeled the spike and drag induced by the broadening of the spike tip to find that that the resulting drag had a strong effect on the spike penetration.

The objective of this work is to use numerical simulations to investigate two-dimensional planar blast waves interacting with perturbed gas interfaces. The resulting interaction gives rise to Richtmyer-Meshkov and Rayleigh-Taylor growth, depending on the shock strength and blast profile. Specifically, we want to identify regimes

in which one or the other instability dominates. We seek to provide models of the perturbation growth and vorticity production mechanisms for two configurations. In contrast with previous studies, we analyze two different configurations: one in which the blast wave goes from a heavy fluid to a lighter one (Rayleigh-Taylor unstable configuration), and vice-versa (Rayleigh-Taylor stable configuration). Our analysis is based on simulations of a two-dimensional planar blast wave, modeled by a shock (instantaneous acceleration) followed by a rarefaction (time-dependent deceleration), interacting with a sinusoidal perturbation at an interface between two fluids. Our blast wave model is such that we can control the shock front Mach number, the rarefaction strength and the rarefaction length. Varying these three parameters, as well as the configuration, will enable a rigorous exploration of the instability dynamics. We use a high-order accurate Discontinuous Galerkin method to solve the multifluid Euler equations that model the system.

3.4.2 Proposed work

The chapter will be organized as follows. First, the problem setup, including the fluid properties and blast wave model, are detailed. We then provide some preliminary models of the position, velocity, and acceleration of a one-dimensional interface driven by a blast wave, as well as models for the volumetric expansion or compression of the interface. These models are validated with one-dimensional simulations. Finally, using simulations of two-dimensional blast wave-driven hydrodynamic instabilities, we will develop and validate models of the perturbation growth and vorticity production mechanisms.

3.4.2.1 Problem setup

Domain and fluid properties For the two-dimensional simulations, the domain is one perturbation wavelength-wide, λ, in the x-direction and 50λ long in the y-direction. The $x = 0$ and $x = \lambda$ boundaries are periodic. Non-reflecting boundary conditions, modeled as zero gradient boundary conditions, are used at the ends of the shock tube. The mesh is uniform in x and y and there are 100 cells per wavelength. At this resolution, integral quantities are converged. For the DG method, a linear polynomial basis ($N = 1$) is used to achieve third-order accuracy in smooth regions. A thermodynamically consistent diffuse interface between the gases [102] is initialized using an exponential diffusion function with an initial thickness of 0.08λ. To measure the mixing layer width, the reported perturbation amplitude is the half difference between the $x = 0$ and $x = 0.5\lambda$ interface locations. The location of the perturbation is defined as the 0.5 contour level of the mass fraction field. The initial perturbation amplitude, a_0, is 0.03λ.

Our problem consists of a blast wave propagating downwards to interact with with an initially perturbed interface separating two gases A and B of different densities and $\gamma = 1.4$, Figure 3.9. The density of the top fluid ρ_A, is the reference density and the density of the bottom fluid, ρ_B, is either $3\rho_A$ or $\frac{1}{3}\rho_A$. This corresponds to two configurations: a light fluid on top of a heavy one where the Atwood number

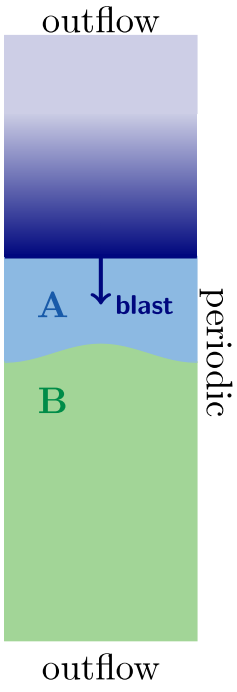

Figure 3.9: Problem setup.

$A = \frac{\rho_A - \rho_B}{\rho_A + \rho_B} = -0.5$, and a heavy fluid on top of a light one where $A = 0.5$.

Modeling the blast wave The blast wave is modeled as a shock followed by a rarefaction, Figure 3.10. This flexible initialization was chosen to provide precise control over the blast front Mach number, M_s, blast wave strength, K, and blast wave length when it reaches the interface, L. We denote the region ahead of the shock with a subscript 0, the post-shock/pre-rarefaction region with 1, the rarefaction region with r, and the post-rarefaction region with 2. The shock is located at x_s, the head of the rarefaction is at x_h and the tail is at x_t. The shock and the rarefaction are both moving towards the left. The distance between the initial positions of the shock and the following rarefaction is such that the rarefaction reaches the interfaces at the same time as the shock, i.e. $x_s = x_h = x_i$ at t_i, where x_i is the interface location and t_i is the time of interaction between the blast wave and the interface.

In the post-shock region, given a Mach number, the shock relations determine ρ, u, and p:

$$\frac{\rho_1}{\rho_0} = \frac{(\gamma+1)M_s^2}{(\gamma-1)M_s^2+2}, \tag{3.1a}$$

$$u_1 = 1 - \frac{\rho_0}{\rho_1}u_s, \tag{3.1b}$$

$$\frac{p_1}{p_0} = \frac{2\gamma M_s^2 - (\gamma-1)}{\gamma+1}, \tag{3.1c}$$

where the shock velocity $u_s = -M_s c_0$. The shock position is $x_s(t) = u_s t + x_{s0}$ where

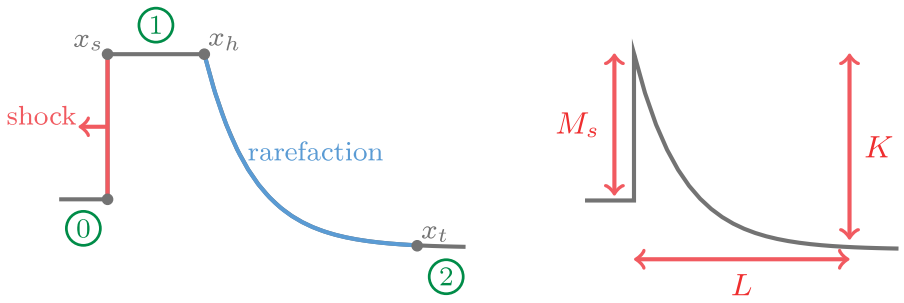

(a) (b)

Figure 3.10: Schematics of (a) initial modeled blast wave profile and (b) modeled blast wave profile at interface interaction time, t_i, with the problem parameters: the blast wave length, L, the rarefaction strength, K, and the blast front Mach number, M_s.

x_{s0} is the shock origin.

The strength of the rarefaction, K, is defined as $K = \frac{p_2}{p_1}$ and determines the flow conditions in region 2:

$$\frac{\rho_2}{\rho_1} = K^{\frac{1}{\gamma}}, \tag{3.2a}$$

$$u_2 = \frac{2c_1}{\gamma - 1}\left(1 - K^{\frac{\gamma-1}{2\gamma}}\right) + u_1, \tag{3.2b}$$

The rarefaction is moving into a flow moving at the post-shock velocity u_1. Inside the rarefaction, we have

$$\frac{\rho_r}{\rho_1} = \left(1 - \frac{\gamma - 1}{2}\frac{|u_r - u_1|}{c_1}\right)^{\frac{2}{\gamma-1}}, \tag{3.3a}$$

$$u_r = \frac{2}{\gamma + 1}\left(c_1 - u_1 + \frac{x - x_{r0}}{t}\right) + u_1, \tag{3.3b}$$

$$\frac{p_r}{p_1} = \left(1 - \frac{\gamma - 1}{2}\frac{|u_r - u_1|}{c_1}\right)^{\frac{2\gamma}{\gamma-1}}, \tag{3.3c}$$

where x_{r0} is the rarefaction origin. The rarefaction head location is $x_h = -(c_1 - u_1)t + x_{r0}$ and the tail location is $x_t = -\left(c_1 - u_1 - \frac{\gamma+1}{2}(u_2 - u_1)\right)t + x_{r0}$. The length of the rarefaction is therefore $|x_h - x_t| = \frac{\gamma+1}{2}(u_2 - u_1)t$. Given M_s, K, and L, we can determine x_{s0} and x_{r0} such that the shock and rarefaction coalesce to form a blast wave as they reach the interface. The time at which a rarefaction of length L reaches the interface is $t_i = \frac{2}{\gamma+1}\frac{L}{u_2 - u_1}$. Using t_i, we can solve for the shock and rarefaction origins:

$$x_i = x_s(t_i) \quad \Rightarrow \quad x_{s0} = x_i - u_s t_i, \tag{3.4a}$$

$$x_i = x_h(t_i) \quad \Rightarrow \quad x_{r0} = x_i + (c_1 - u_1)t_i. \tag{3.4b}$$

The simulations are initialized at $t_0 = 0.5t_i$. This setup provides similar Mach number decay rates and blast profiles as the point blast initialization, Figure 3.11, and allows us to explicitly control the shock Mach number, the rarefaction length, and the rarefaction strength.

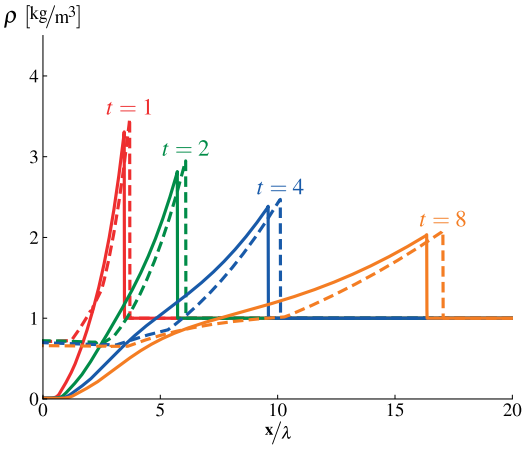

(a) Density profile of the blast wave as a function of time.

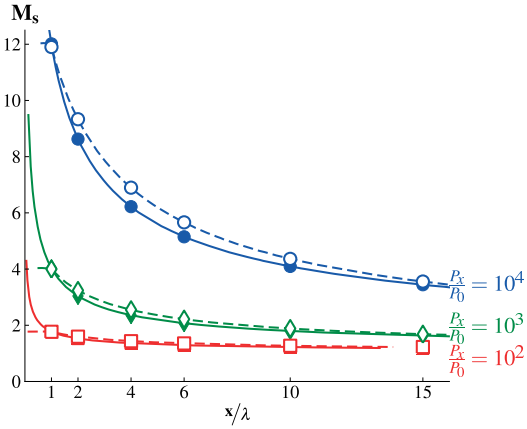

(b) Decay of the shock front Mach number as a function of distance traveled by the blast wave for different initial blast pressure ratios.

Figure 3.11: Comparison of the density profile and shock Mach number for a blast wave initialized by a localized deposition of energy and our model of the blast wave using a shock and a rarefaction. Solid lines and symbols: point-source blast wave; dashed lines and empty symbols: model blast wave.

3.4.2.2 Volumetric expansions of blast waves at interfaces

As the blast wave traverses the material, it changes the material volume by compressing it first (the shock front) and decompressing it (the following rarefaction). Volumetric changes will have an effect on the growth of the perturbation. Our models for volumetric changes will be useful in determining the decompression effects on the two-dimensional perturbation growth.

We start by analyzing the volumetric expansion associated to a pure rarefaction interacting with an interface. Using simple wave theory of gas dynamics, we can explicitly solve the gas state post-rarefaction interaction. Assuming a pure rarefaction interacting with a gas-gas interface, with the rarefaction initialized in the A medium and moving into the B medium, the isentropic relations state that the ratio of sound speeds pre and post rarefaction interaction is

$$\frac{c_{Ar}}{c_A} = 1 - T\frac{\gamma - 1}{2}\frac{u_2}{c_A} \tag{3.5a}$$

$$\frac{c_{Br}}{c_B} = 1 - T\frac{\gamma - 1}{2}\frac{u_2}{c_A} \tag{3.5b}$$

where c_A is the initial sound speed in the A medium, c_{Ar} the sound speed in medium A after rarefaction interaction, c_B the initial sound speed in the B medium, c_{Br} the sound speed in medium B after rarefaction interaction, $T = \frac{2\alpha}{\alpha+1}$ the transmission coefficient ($\alpha = \frac{c_A}{c_B}$). By combining the isentropic relations and the expression relating the sound speed to temperature, we have

$$\frac{p_{Br}}{p_0} = \left(\frac{c_{Br}}{c_B}\right)^{\frac{2\gamma}{\gamma-1}} \tag{3.6a}$$

$$\frac{\rho_{Br}}{\rho_B} = \left(\frac{c_{Br}}{c_B}\right)^{\frac{2}{\gamma-1}} \tag{3.6b}$$

and similarly for material A. Therefore, the associated volume change due to the passage of the rarefaction is

$$V_{Br} = V_B \left(\frac{p_{Br}}{p_0}\right)^{\frac{-1}{\gamma}} \quad \text{and} \quad V_{Ar} = V_A \left(\frac{p_{Ar}}{p_0}\right)^{\frac{-1}{\gamma}}. \tag{3.7a}$$

For a blast wave, we must take into account the effect of the shock. There are two situations: if the blast is going from a light gas into a heavier one, there will be a reflected and transmitted shock; if the blast is going from a heavy gas into a lighter one, there will be a reflected rarefaction and a transmitted shock. These situations are qualitatively different and the reflected wave is going to interact differently with the incoming rarefaction wave (the main part of the blast wave). We are currently developing models to take into account the effect of these reflected waves interacting with the incoming wave. For the second case, where a rarefaction is reflected by the interface, we can again use simple wave theory, assume isentropic flow, and solve the interaction between two rarefactions. The effect of the reflected rarefaction is to increase the strength of the rarefaction (because of decompression effects). We have implemented this model and obtain good agreement (within 15%) when compared to one-dimensional numerical simulations.

3.4.2.3 Modeling the growth dynamics of blast driven-hydrodynamic instabilities

We are currently exploring existing growth models for the blast-driven instability. The most common model for the non-linear stage of the Rayleigh-Taylor instability with a time varying acceleration field is a buoyancy-drag model detailed in [17],

$$(\rho_b + C_a\rho_s)\frac{\mathrm{d}u_b}{\mathrm{d}t} = (\rho_s - \rho_b)g(t) - \frac{C_d}{\lambda}\rho_s u_b^2 \tag{3.8a}$$

where ρ_b is the bubble density, ρ_s the spike density, u_b the bubble velocity with respect to the one-dimensional interface, C_a the added mass coefficient ($C_a = 2$ in two dimensions), and C_d the drag coefficient ($C_d = 6\pi$ in two dimensions). The model has some success describing the bubble evolution in the non-linear stages of

the perturbation growth. Srebro et al. [96] proposed the addition of a dependence on the amplitude growth to model the early-mid-late stages of the growth through a term, $E(t) = \exp(-C_e k h_b)$, where h_b is the bubble height, $k = \frac{2\pi}{\lambda}$, and $C_e = 3$ in two dimensions. The bubble growth model then becomes

$$((C_a E(t) + 1)\rho_b + (C_a + E(t))\rho_s)\frac{\mathrm{d}u_b}{\mathrm{d}t} = (1 - E(t))(\rho_s - \rho_b)g(t) - \frac{C_d}{\lambda}\rho_s u_b^2. \tag{3.9a}$$

In the linear growth stage, a first order expansion about h_b reduces this model to

$$\frac{\mathrm{d}u_b}{\mathrm{d}t} = Akh_b g(t). \tag{3.10a}$$

For the blast driven-hydrodynamic instability, Miles [97] used the initial buoyancy-drag model and added a term to the bubble height, h_b, given by the volumetric expansion of the material due to the blast wave passage. The volumetric expansion was based on one-dimensional simulations. We propose to use the models developed in Section 3.4.2.2 in place of one-dimensional simulations. Preliminary comparisons with our simulations show that existing models may not be capturing all the growth dynamics. Changes in the bubble and spike densities may need to be accommodated into the existing buoyancy-drag models. For the post-blast wave growth phase, buoyancy-drag models fail to capture the growth dynamics as the acceleration field is zero. The growth of the perturbation is driven solely by the baroclinic vorticity generated at the interface by the blast wave. To capture this growth phase we are therefore also exploring circulation-based growth models using approaches similar to Jacobs and Sheeley [8].

CHAPTER IV

Conclusions and Future Work

The objective of this work is (i) to develop a numerical and computational framework to perform studies of mixing phenomena in compressible multiphase flows, and (ii) to study mixing phenomena relevant to many scientific and engineering applications, including inertial confinement fusion, supernova explosions, fuel injection, plasma deposition, cancer treatments, and turbomachinery.

To accomplish our first objective,

- we presented novel numerical techniques to solve consistently compressible multiphase flows with shocks and interfaces [103, 58];
- we implemented a multi-GPU parallel paradigm to resolve the flow features and the length scales of interest by combining the CUDA framework and the Message Passing Interface to communicate between GPUs [104];

Using this framework, we have also addressed our second objective by

- studying the mixing dynamics of multi-layered Richtmyer-Meshkov instabilities and providing support to the idea that shocks and rarefactions can be used to control the instability growth [105];
- using the Rayleigh-Taylor instability to test material strength models of Beryllium in high-strain-rate and pressure regimes [106];
- providing insights into the flow dynamics of the blast-driven Kelvin-Helmholtz instability, which were subsequently used to model experiments in [107];
- analyzing the interactions between a supersonic gas flow and a compliant water cylinder and their effects on the wake dynamics [104].

Finally, to complete the doctoral thesis, we propose to accomplish the following objectives:

1. provide growth models for the blast wave-driven hydrodynamic instability at different strengths, lengths, and configurations (present to November 2015);
    - comparison of simulation growth to existing blast wave instability models;

- incorporate time varying density in the bubble and spike into models;
- model the post-blast wave interaction phase using circulation and vorticy deposition models.

2. study the physical mechanisms driving the breakup of a supersonic liquid drop (November 2015 to March 2016);
   - understand the coupling between a compliant body, the liquid drop, and a supersonic air flow.
   - study the baroclinic vorticity deposition due to the shock passage and model the droplet dynamics using vortex sheet models.
   - quantify the effect of the reentrant flow on the drop spreading.
3. improve the accuracy of the discontinuous Galerkin method's discretization of the advection terms and study the method's robustness to random errors, which could occur in high performance computing clusters due to bit-flipping or broken transistors (November 2015 to March 2016);
4. use our computational framework to study the supersonic bubbly flow over a wedge and compare the results to experiments conducted by Prof. Ceccio's research group (present - March 2016).

BIBLIOGRAPHY

BIBLIOGRAPHY

[1] R. D. Richtmyer, Taylor instability in shock acceleration of compressible fluids, Commun. Pure Appl. Math. 13 (1960) 297–319.

[2] E. E. Meshkov, Instability of the interface of two gases accelerated by a shock wave, Fluid Dyn. 4 (1969) 101–104.

[3] M. Brouillette, The Richtmyer–Meshkov Instability, Ann. Rev. Fluid Mech. 34 (2002) 445–468.

[4] K. a. Meyer, Numerical Investigation of the Stability of a Shock-Accelerated Interface between Two Fluids, Phys. Fluids 15 (1972) 753.

[5] Q. Zhang, S.-I. Sohn, Nonlinear theory of unstable fluid mixing driven by shock wave, Phys. Fluids 9 (1997) 1106.

[6] O. Sadot, L. Erez, U. Alon, D. Oron, L. A. Levin, G. Erez, G. Ben-Dor, D. Shvarts, Study of Nonlinear Evolution of Single-Mode and Two-Bubble Interaction under Richtmyer-Meshkov Instability, Phys. Rev. Lett. 80 (1998) 1654–1657.

[7] R. Samtaney, N. J. Zabusky, Circulation deposition on shock-accelerated planar and curved density-stratified interfaces: models and scaling laws, J. Fluid Mech. 269 (1994) 45.

[8] J. W. Jacobs, J. M. Sheeley, Experimental study of incompressible Richtmyer–Meshkov instability, Phys. Fluids 8 (1996) 405.

[9] G. Taylor, The Instability of Liquid Surfaces when Accelerated in a Direction Perpendicular to their Planes. I, Proc. R. Soc. A Math. Phys. Eng. Sci. 201 (1950) 192–196.

[10] R. E. Duff, F. H. Harlow, C. W. Hirt, Effects of Diffusion on Interface Instability between Gases, Phys. Fluids 5 (1962) 417.

[11] K. Read, Experimental investigation of turbulent mixing by Rayleigh-Taylor instability, Phys. D Nonlinear Phenom. 12 (1984) 45–58.

[12] S. B. Dalziel, P. F. Linden, D. L. Youngs, Self-similarity and internal structure of turbulence induced by Rayleigh–Taylor instability, J. Fluid Mech. 399 (1999) S002211209900614X.

[13] G. Dimonte, M. Schneider, Density ratio dependence of Rayleigh–Taylor mixing for sustained and impulsive acceleration histories, Phys. Fluids 12 (2000) 304.

[14] G. Dimonte, D. L. Youngs, A. Dimits, S. Weber, M. Marinak, S. Wunsch, C. Garasi, A. Robinson, M. J. Andrews, P. Ramaprabhu, a. C. Calder, B. Fryxell, J. Biello, L. Dursi, P. MacNeice, K. Olson, P. Ricker, R. Rosner, F. Timmes, H. Tufo, Y.-N. Young, M. Zingale, A comparative study of the turbulent Rayleigh–Taylor instability using high-resolution three-dimensional numerical simulations: The Alpha-Group collaboration, Phys. Fluids 16 (2004) 1668.

[15] P. Ramaprabhu, G. Dimonte, Y.-N. Young, a. C. Calder, B. Fryxell, Limits of the potential flow approach to the single-mode Rayleigh-Taylor problem, Phys. Rev. E 74 (2006) 066308.

[16] P. Ramaprabhu, G. Dimonte, P. Woodward, C. Fryer, G. Rockefeller, K. Muthuraman, P.-H. Lin, J. Jayaraj, The late-time dynamics of the single-mode Rayleigh-Taylor instability, Phys. Fluids 24 (2012) 074107.

[17] D. Oron, L. Arazi, D. Kartoon, A. Rikanati, U. Alon, D. Shvarts, Dimensionality dependence of the Rayleigh–Taylor and Richtmyer–Meshkov instability late-time scaling laws, Phys. Plasmas 8 (2001) 2883.

[18] A. R. Miles, M. J. Edwards, B. Blue, J. F. Hansen, H. F. Robey, R. P. Drake, C. Kuranz, D. R. Leibrandt, The effect of a short-wavelength mode on the evolution of a long-wavelength perturbation driven by a strong blast wave, Phys. Plasmas 11 (2004) 5507.

[19] C. C. Kuranz, R. P. Drake, E. C. Harding, M. J. Grosskopf, H. F. Robey, B. a. Remington, M. J. Edwards, a. R. Miles, T. S. Perry, B. E. Blue, T. Plewa, N. C. Hearn, J. P. Knauer, D. Arnett, D. R. Leibrandt, TWO-DIMENSIONAL BLAST-WAVE-DRIVEN RAYLEIGH-TAYLOR INSTABILITY: EXPERIMENT AND SIMULATION, Astrophys. J. 696 (2009) 749–759.

[20] A. W. Cook, P. E. Dimotakis, Transition stages of Rayleigh–Taylor instability between miscible fluids, J. Fluid Mech. 443 (2001) 69–99.

[21] K.-H. Kim, G. Chahine, J.-P. Franc, A. Karimi (Eds.), Advanced Experimental and Numerical Techniques for Cavitation Erosion Prediction, volume 106 of *Fluid Mechanics and Its Applications*, Springer Netherlands, Dordrecht, 2014.

[22] J. C. Meng, T. Colonius, Numerical simulations of the early stages of high-speed droplet breakup, Shock Waves (2014) 399–414.

[23] P. Welch, P. Boyle, New turbines to Enable Efficient Geothermal Power Plants, Geotherm. Resour. Counc. Trans. 33 (2009) 8.

[24] T. Theofanous, Aerobreakup of Newtonian and Viscoelastic Liquids, Annu. Rev. Fluid Mech. 43 (2011) 661–690.

[25] K. K. Haller, Y. Ventikos, D. Poulikakos, P. Monkewitz, Computational study of high-speed liquid droplet impact, J. Appl. Phys. 92 (2002) 2821–2828.

[26] K. K. Haller, D. Poulikakos, Y. Ventikos, P. Monkewitz, Shock wave formation in droplet impact on a rigid surface: lateral liquid motion and multiple wave structure in the contact line region, J. Fluid Mech. 490 (2003) 1–14.

[27] L. Bayvel, Z. Orzechowski, Liquid Atomization, Taylor and Francis, Washington, DC, 1993.

[28] J. Yang, T. Kubota, E. E. Zukoski, Applications of shock-induced mixing to supersonic combustion, AIAA J. 31 (1993) 854–862.

[29] E. Johnsen, Benchmark multifluid problems (2008) 1–11.

[30] E. Vlaisavljevich, A. Maxwell, M. Warnez, E. Johnsen, C. a. Cain, Z. Xu, Histotripsy-Induced Cavitation Cloud Mechanical Properties, IEEE Trans. Ultrason. Ferroelectr. Freq. Control 61 (2014) 341–352.

[31] K. M. Case, Taylor Instability of an Inverted Atmosphere, Phys. Fluids 3 (1960) 366.

[32] H. Michioka, Rayleigh-Taylor instability of a particle packed viscous fluid: Implications for a solidifying magma, Geophys. Res. Lett. 32 (2005) L03309.

[33] M. K. Davey, J. a. Whitehead, Rotating rayleigh-taylor instability as a model of sinking events in the ocean, Geophys. Astrophys. Fluid Dyn. 17 (1981) 237–253.

[34] M. Cuk, S. T. Stewart, Making the Moon from a Fast-Spinning Earth: A Giant Impact Followed by Resonant Despinning, Science (80-.). 338 (2012) 1047–1052.

[35] J. Lindl, Development of the indirect-drive approach to inertial confinement fusion and the target physics basis for ignition and gain, Phys. Plasmas 2 (1995) 3933.

[36] J. D. Lawson, Some Criteria for a Power Producing Thermonuclear Reactor, Proc. Phys. Soc. Sect. B 70 (1957) 6–10.

[37] O. L. Landen, R. Benedetti, D. Bleuel, T. R. Boehly, D. K. Bradley, J. a. Caggiano, D. a. Callahan, P. M. Celliers, C. J. Cerjan, D. Clark, G. W. Collins, E. L. Dewald, S. N. Dixit, T. Doeppner, D. Edgell, J. Eggert, D. Farley, J. a. Frenje, V. Glebov, S. M. Glenn, S. H. Glenzer, S. W. Haan, A. Hamza, B. a. Hammel, C. a. Haynam, J. H. Hammer, R. F. Heeter, H. W. Herrmann, D. G. Hicks, D. E. Hinkel, N. Izumi, M. Gatu Johnson, O. S. Jones, D. H. Kalantar, R. L. Kauffman, J. D. Kilkenny, J. L. Kline, J. P. Knauer, J. a. Koch, G. a. Kyrala, K. LaFortune, T. Ma, a. J. Mackinnon, a. J. Macphee, E. Mapoles, J. L. Milovich, J. D. Moody, N. B. Meezan, P. Michel, a. S. Moore, D. H. Munro, A. Nikroo, R. E. Olson, K. Opachich, A. Pak, T. Parham, P. Patel, H.-S. Park,

R. P. Petrasso, J. Ralph, S. P. Regan, B. a. Remington, H. G. Rinderknecht, H. F. Robey, M. D. Rosen, J. S. Ross, J. D. Salmonson, T. C. Sangster, M. B. Schneider, V. Smalyuk, B. K. Spears, P. T. Springer, L. J. Suter, C. a. Thomas, R. P. J. Town, S. V. Weber, P. J. Wegner, D. C. Wilson, K. Widmann, C. Yeamans, A. Zylstra, M. J. Edwards, J. D. Lindl, L. J. Atherton, W. W. Hsing, B. J. MacGowan, B. M. Van Wonterghem, E. I. Moses, Progress in the indirect-drive National Ignition Campaign, Plasma Phys. Control. Fusion 54 (2012) 124026.

[38] R. P. Drake, High-Energy-Density Physics, Spring-Verlag, Berlin, 2006.

[39] F. Hoyle, On Nuclear Reactions Occuring in Very Hot STARS.I. the Synthesis of Elements from Carbon to Nickel., Astrophys. J. Suppl. Ser. 1 (1954) 121.

[40] S. E. Woosley, W. D. Arnett, D. D. Clayton, The Explosive Burning of Oxygen and Silicon, Astrophys. J. Suppl. Ser. 26 (1973) 231.

[41] P. a. Seeger, W. a. Fowler, D. D. Clayton, Nucleosynthesis of Heavy Elements by Neutron Capture., Astrophys. J. Suppl. Ser. 11 (1965) 121.

[42] C. L. Fryer, K. C. New, Gravitational Waves from Gravitational Collapse, Living Rev. Relativ. 14 (2011).

[43] R. Abgrall, How to Prevent Pressure Oscillations in Multicomponent Flow Calculations: A Quasi Conservative Approach, J. Comput. Phys. 125 (1996) 150–160.

[44] K.-M. Shyue, An Efficient Shock-Capturing Algorithm for Compressible Multicomponent Problems, J. Comput. Phys. 142 (1998) 208–242.

[45] E. Johnsen, F. Ham, Preventing numerical errors generated by interface-capturing schemes in compressible multi-material flows, J. Comput. Phys. 231 (2012) 5705–5717.

[46] S. Adjerid, K. D. Devine, J. E. Flaherty, L. Krivodonova, A posteriori error estimation for discontinuous Galerkin solutions of hyperbolic problems, Comput. Methods Appl. Mech. Eng. 191 (2002) 1097–1112.

[47] S. Adjerid, T. C. Massey, Superconvergence of discontinuous Galerkin solutions for a nonlinear scalar hyperbolic problem, Comput. Methods Appl. Mech. Eng. 195 (2006) 3331–3346.

[48] B. Cockburn, G. Lin, C.-W. Shu, TVB Runge-Kutta local projection discontinuous Galerkin finite element method for conservation laws III: One-dimensional systems, J. Comput. Phys. 84 (1989) 90–113.

[49] B. Cockburn, C.-W. Shu, TVB Runge-Kutta Local Projection Discontinuous Galerkin Finite Element Method for Conservation Laws II: General Framework, Math. Comput. 52 (1989) 411–435.

[50] B. Cockburn, S. Hou, C.-W. Shu, The Runge-Kutta local projection discontinuous Galerkin finite element method for conservation laws IV: The multidimensional case, Math. Comput. 54 (1990) 545–581.

[51] B. Cockburn, C.-W. Shu, The Local Discontinuous Galerkin Method for Time-Dependent Convection-Diffusion Systems, SIAM J. Numer. Anal. 35 (1997) 2440–2463.

[52] B. Cockburn, C.-W. Shu, The Runge-Kutta Discontinuous Galerkin Method for Conservation Laws V: Multidimensional Systems, J. Comput. Phys. 141 (1997) 199–224.

[53] R. Biswas, K. D. Devine, J. E. Flaherty, Parallel, adaptive finite element methods for conservation laws, Appl. Numer. Math. 14 (1994) 255–283.

[54] L. Krivodonova, Limiters for high-order discontinuous Galerkin methods, J. Comput. Phys. 226 (2007) 879–896.

[55] D. Kuzmin, A vertex-based hierarchical slope limiter for -adaptive discontinuous Galerkin methods, J. Comput. Appl. Math. 233 (2010) 3077–3085.

[56] Y. Liu, C.-W. Shu, E. Tadmor, M. Zhang, Central Discontinuous Galerkin Methods on Overlapping Cells with a Nonoscillatory Hierarchical Reconstruction, SIAM J. Numer. Anal. 45 (2007) 2442.

[57] Z. Xu, Y. Liu, C.-W. Shu, Hierarchical reconstruction for discontinuous Galerkin methods on unstructured grids with a WENO-type linear reconstruction and partial neighboring cells, J. Comput. Phys. 228 (2009) 2194–2212.

[58] M. T. Henry de Frahan, S. Varadan, E. Johnsen, A new limiting procedure for discontinuous Galerkin methods applied to compressible multiphase flows with shocks and interfaces, J. Comput. Phys. 280 (2015) 489–509.

[59] D. N. Arnold, F. Brezzi, B. Cockburn, L. D. Marini, Unified Analysis of Discontinuous Galerkin Methods for Elliptic Problems, SIAM J. Numer. Anal. 39 (2002) 1749–1779.

[60] F. Brezzi, G. Manzini, D. Marini, P. Pietra, A. Russo, Discontinuous Galerkin approximations for elliptic problems, Numer. Methods Partial Differ. Equ. 16 (2000) 365–378.

[61] J. Douglas, T. Dupont, Interior penalty procedures for elliptic and parabolic Galerkin methods, Comput. methods Appl. Sci. (1976) 207–216.

[62] F. Bassi, S. Rebay, A High-Order Accurate Discontinuous Finite Element Method for the Numerical Solution of the Compressible Navier–Stokes Equations, J. Comput. Phys. 131 (1997) 267–279.

[63] J. Peraire, P.-O. Persson, The Compact Discontinuous Galerkin (CDG) Method for Elliptic Problems, SIAM J. Sci. Comput. 30 (2007) 25.

[64] M. Lo, B. van Leer, Recovery-Based Discontinuous Galerkin for Navier-Stokes Viscous Terms, AIAA Pap. (2011) AIAA–2011–3406.

[65] B. van Leer, M. Lo, Unification of Discontinuous Galerkin Methods for Advection and Diffusion 1 Introduction : history of RDG, New Horizons (2009) 1–12.

[66] B. van Leer, M. Lo, A Discontinuous Galerkin Method for Diffusion Based on Recovery, Fluid Dyn. (2007).

[67] L. H. Khieu, E. Johnsen, Analysis of Improved Advection Schemes for Discontinuous Galerkin Methods, in: 7th AIAA Theor. Fluid Mech. Conf., June, American Institute of Aeronautics and Astronautics, Reston, Virginia, 2014, pp. 1–14.

[68] B. Bishop, New experimental research exposes the strength of beryllium at extreme conditions, 2015.

[69] D. Igra, K. Takayama, Investigation of aerodynamic breakup of a cylindrical water droplet, At. Sprays (2001).

[70] D. Igra, K. Takayama, Experimental Investigation of Two Cylindrical Water Columns Subjected to Planar Shock Wave Loading, J. Fluids Eng. 125 (2003) 325.

[71] J. Meng, T. Colonius, Droplet Breakup in High-Speed Gas Flows, in: 8th Int. Conf. Multiph. Flow, 2011, ICMF, Jeju, Korea, 2013.

[72] G. Dimonte, Nonlinear evolution of the Rayleigh–Taylor and Richtmyer–Meshkov instabilities, Phys. Plasmas 6 (1999) 2009.

[73] B. Fryxell, D. Arnett, E. Mueller, Instabilities and clumping in SN 1987A. I - Early evolution in two dimensions, Astrophys. J. 367 (1991) 619.

[74] G. Taylor, The Formation of a Blast Wave by a Very Intense Explosion. I. Theoretical Discussion, Proc. R. Soc. A Math. Phys. Eng. Sci. 201 (1950) 159–174.

[75] L. I. Sedov, Propagation of strong shock waves, J. Appl. Math. Mech. 10 (1946) 241–250.

[76] X. Ribeyre, V. T. Tikhonchuk, S. Bouquet, Compressible Rayleigh–Taylor instabilities in supernova remnants, Phys. Fluids 16 (2004) 4661.

[77] K. Kifonidis, T. Plewa, L. Scheck, H.-T. Janka, E. Müller, Non-spherical core collapse supernovae, Astron. Astrophys. 453 (2006) 661–678.

[78] P. J. McGregor, P. D. Nicholson, M. G. Allen, CASPIR Observations of the Collision of Comet Shoemaker–Levy 9 with Jupiter, Icarus 121 (1996) 361–388.

[79] L. Rayleigh, Aerial Plane Waves of Finite Amplitude, Proc. R. Soc. A Math. Phys. Eng. Sci. 84 (1910) 247–284.

[80] D. Sharp, An overview of Rayleigh-Taylor instability, Phys. D Nonlinear Phenom. 12 (1984) 3–18.

[81] W. H. Cabot, A. W. Cook, Reynolds number effects on Rayleigh–Taylor instability with possible implications for type Ia supernovae, Nat. Phys. 2 (2006) 562–568.

[82] R. P. Drake, D. R. Leibrandt, E. C. Harding, C. C. Kuranz, M. a. Blackburn, H. F. Robey, B. a. Remington, M. J. Edwards, a. R. Miles, T. S. Perry, R. J. Wallace, H. Louis, J. P. Knauer, D. Arnett, Nonlinear mixing behavior of the three-dimensional Rayleigh–Taylor instability at a decelerating interface, Phys. Plasmas 11 (2004) 2829.

[83] C. C. Kuranz, R. P. Drake, M. J. Grosskopf, B. Fryxell, A. Budde, J. F. Hansen, a. R. Miles, T. Plewa, N. Hearn, J. Knauer, Spike morphology in blast-wave-driven instability experiments, Phys. Plasmas 17 (2010) 052709.

[84] A. R. Miles, M. J. Edwards, J. A. Greenough, Effect of initial conditions on two-dimensional Rayleigh–Taylor instability and transition to turbulence in planar blast-wave-driven systems, Phys. Plasmas 11 (2004) 5278.

[85] a. R. Miles, B. Blue, M. J. Edwards, J. a. Greenough, J. F. Hansen, H. F. Robey, R. P. Drake, C. Kuranz, D. R. Leibrandt, Transition to turbulence and effect of initial conditions on three-dimensional compressible mixing in planar blast-wave-driven systems, Phys. Plasmas 12 (2005) 056317.

[86] A. R. Miles, THE BLAST-WAVE-DRIVEN INSTABILITY AS A VEHICLE FOR UNDERSTANDING SUPERNOVA EXPLOSION STRUCTURE, Astrophys. J. 696 (2009) 498–514.

[87] K. Mori, Two-fluid simulations of shock wave propagation and shock-bubble interaction in collisionless plasma, Phys. Plasmas 19 (2012) 032311.

[88] N. Zabusky, J. Ray, R. S. Samtaney, Vortex Models for Richtmyer – Meshkov Fast / Slow Environments : Scaling Laws for Interface Growth Rates, in: R. Young, J. Glimm, B. Boyton (Eds.), Proc. 5th Int. Work. Compressible Turbul. Mix., World Scientific, Singapore, 1996, pp. 89–97.

[89] N. J. Zabusky, VORTEX PARADIGM FOR ACCELERATED INHOMOGENEOUS FLOWS: Visiometrics for the Rayleigh-Taylor and Richtmyer-Meshkov Environments, Annu. Rev. Fluid Mech. 31 (1999) 495–536.

[90] a. Rikanati, U. Alon, D. Shvarts, Vortex model for the nonlinear evolution of the multimode Richtmyer-Meshkov instability at low Atwood numbers, Phys. Rev. E 58 (1998) 7410–7418.

[91] R. L. Holmes, G. Dimonte, B. Fryxell, M. L. Gittings, J. W. Grove, M. Schneider, D. H. Sharp, A. L. Velikovich, R. P. Weaver, Q. Zhang, Richtmyer–Meshkov instability growth: experiment, simulation and theory, J. Fluid Mech. 389 (1999) 55–79.

[92] A. D. Kotelnikov, N. J. Zabusky, Vortex Dynamics of a Twice-accelerated Interface in an Incompressible Ideal Fluid, Astrophys. J. Suppl. Ser. 127 (2000) 389–394.

[93] G. Peng, N. J. Zabusky, S. Zhang, Vortex-accelerated secondary baroclinic vorticity deposition and late-intermediate time dynamics of a two-dimensional Richtmyer–Meshkov interface, Phys. Fluids 15 (2003) 3730.

[94] a. Rikanati, D. Oron, O. Sadot, D. Shvarts, High initial amplitude and high Mach number effects on the evolution of the single-mode Richtmyer-Meshkov instability, Phys. Rev. E 67 (2003) 026307.

[95] R. V. Morgan, R. Aure, J. D. Stockero, J. a. Greenough, W. Cabot, O. a. Likhachev, J. W. Jacobs, On the late-time growth of the two-dimensional Richtmyer–Meshkov instability in shock tube experiments, J. Fluid Mech. 712 (2012) 354–383.

[96] Y. Srebro, Y. Elbaz, O. Sadot, L. Arazi, D. Shvarts, A general buoyancy–drag model for the evolution of the Rayleigh–Taylor and Richtmyer–Meshkov instabilities, Laser Part. Beams 21 (2003) 347–353.

[97] a. R. Miles, Bubble merger model for the nonlinear Rayleigh–Taylor instability driven by a strong blast wave, Phys. Plasmas 11 (2004) 5140.

[98] A. R. Miles, Nonlinear Rayleigh–Taylor instabilities in fast Z pinches, Phys. Plasmas 16 (2009) 032702.

[99] V. N. Goncharov, Analytical model of nonlinear, single-mode, classical Rayleigh-Taylor instability at arbitrary Atwood numbers., Phys. Rev. Lett. 88 (2002) 134502.

[100] K. Mikaelian, Nonlinear hydrodynamic interface instabilities driven by time-dependent accelerations, Phys. Rev. E 79 (2009) 065303.

[101] R. P. Drake, SPIKE PENETRATION IN BLAST-WAVE-DRIVEN INSTABILITIES, Astrophys. J. 744 (2012) 184.

[102] M. Latini, O. Schilling, W. S. Don, Effects of WENO flux reconstruction order and spatial resolution on reshocked two-dimensional Richtmyer–Meshkov instability, J. Comput. Phys. 221 (2007) 805–836.

[103] M. T. Henry de Frahan, E. Johnsen, Discontinuous Galerkin method for multifluid Euler equations, in: 21st AIAA Comput. Fluid Dyn. Conf., American Institute of Aeronautics and Astronautics, Reston, Virginia, 2013, pp. 1–12.

[104] M. Henry de Frahan, E. Johnsen, High-order Discontinuous Galerkin Methods Applied to Multiphase Flows, in: 22nd AIAA Comput. Fluid Dyn. Conf., June, American Institute of Aeronautics and Astronautics, Reston, Virginia, 2015, pp. 1–14.

[105] M. T. Henry de Frahan, P. Movahed, E. Johnsen, Numerical simulations of a shock interacting with successive interfaces using the Discontinuous Galerkin method: the multilayered Richtmyer–Meshkov and Rayleigh–Taylor instabilities, Shock Waves 25 (2015) 329–345.

[106] M. T. Henry de Frahan, J. L. Belof, R. M. Cavallo, V. a. Raevsky, O. N. Ignatova, A. Lebedev, D. S. Ancheta, B. S. El-dasher, J. N. Florando, G. F. Gallegos, E. Johnsen, M. M. LeBlanc, Experimental and numerical investigations of beryllium strength models using the Rayleigh-Taylor instability, J. Appl. Phys. 117 (2015) 225901.

[107] C. A. Di Stefano, G. Malamud, M. T. Henry de Frahan, C. C. Kuranz, A. Shimony, S. R. Klein, R. P. Drake, E. Johnsen, D. Shvarts, V. a. Smalyuk, D. Martinez, Observation and modeling of mixing-layer development in high-energy-density, blast-wave-driven shear flowa), Phys. Plasmas 21 (2014) 056306.